ANL-4798(Del.)

ARGONNE NATIONAL LABORATORY
P. O. Box 5207
Chicago 80, Illinois

QUARTERLY REPORT FOR

DECEMBER, 1951, JANUARY AND FEBRUARY, 1952

PHYSICS DIVISION

Louis A. Turner, Division Director

March 15, 1952

Preceding Quarterlies:

ANL-4659 March, April and May, 1951
ANL-4680 June, July and August, 1951
ANL-4746 September, October, and November, 1951

Operated by The University of Chicago
under
Contract W-31-109-eng-38

DISCLAIMER

TABLE OF CONTENTS

TABLE OF CONTENTS Contin.:

I. Preliminary Report on Angular Distribution of Scattering of Monoenergetic Neutrons A. S. Langsdorf and M. T. Burgy

The scattering of neutrons has been measured at five angles at four energies for uranium, zirconium, iron, and copper, all relative to the scattering by carbon at the same angle and energy. The neutron source was the Li(p,n) reaction; the spread in energy was about 100 kev.

Two methods of observing the angular distribution were employed. Both methods used the same apparatus shown in Figure 1. One method is called the "external" method, the other the "internal" method. For the former method the scattering sample, as shown in the figure, is in the open, exposed to the forward flux of neutrons from the lithium target. Scattered neutrons are detected when they pass through the collimator hole to the counters. (A plug, not shown in Fig. 1, is placed with its front face about at the "middle" internal scattering sample position so that the whole counter assembly becomes a single high efficiency detecting unit. The plug is a paraffin cylinder 2" diameter by 5½" long.) The angular resolution of the external method is determined by the spread at the scattering sample with respect to the source spot on the lithium target. The spread is about $\pm 15^\circ$ max. or $\pm 10^\circ$ average. Measurements were made in this way at five angles, θ, between 30° and 130°.

The "internal" method is so called because the scattering sample is located inside the collimator and shield, in the beam, near where it goes through the hole in the paraffin block containing the BF_3 counters.[1] As shown in Figure 1, neutrons scattered forward are most efficiently detected with the scatterer located in the vicinity of the position marked "forward".

1. For the internal experiments, the neutron source spot is on the axis of the collimator hole, where the external scatterer would be for the external data, and $\theta = 0$ in Fig. 1.

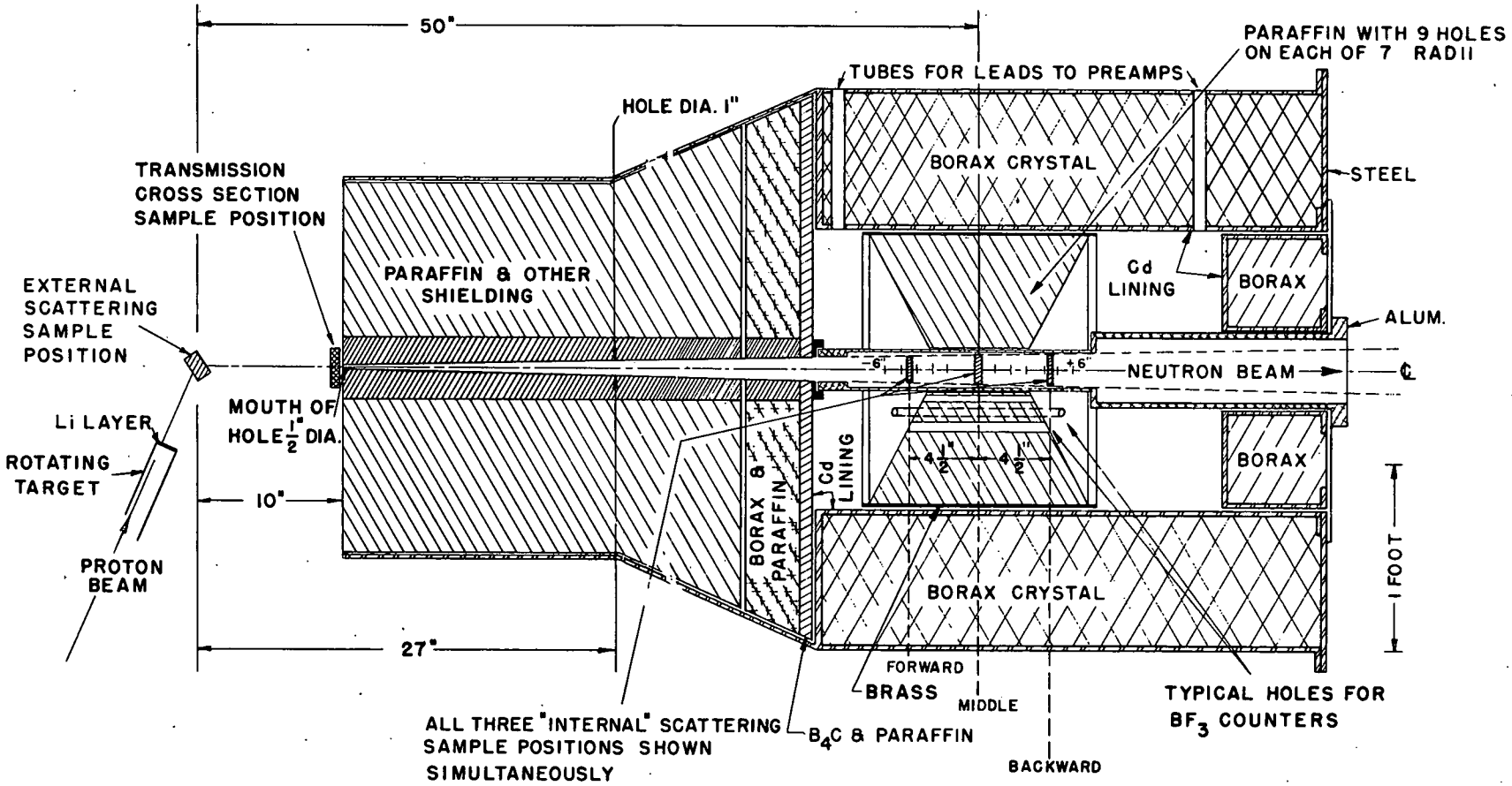
50"
PARAFFIN WITH 9 HOLES ON EACH OF 7 RADII
TUBES FOR LEADS TO PREAMPS
HOLE DIA. 1"
TRANSMISSION CROSS SECTION SAMPLE POSITION
BORAX CRYSTAL
STEEL
PARAFFIN & OTHER SHIELDING
Cd LINING
BORAX
ALUM.
EXTERNAL SCATTERING SAMPLE POSITION
6"
6"
NEUTRON BEAM
Li LAYER
MOUTH OF HOLE 1/2" DIA.
ROTATING TARGET
BORAX & PARAFFIN
Cd LINING
4 1/2"
4 1/2"
BORAX
10"
1 FOOT
PROTON BEAM
BORAX CRYSTAL
27"
FORWARD
BRASS
MIDDLE
TYPICAL HOLES FOR BF3 COUNTERS
ALL THREE "INTERNAL" SCATTERING SAMPLE POSITIONS SHOWN SIMULTANEOUSLY
B4C & PARAFFIN
BACKWARD

Fig. 1

The opposite holds for the "backward" position. In this method the angular spread is very poorly defined, and the actual counting efficiency of the setup as a function of angle is not known at all well. In spite of the crudeness, this technique is a valuable adjunct to the external method: for the internal method the counting rates are higher and give better statistics; background counts are lower, and measurements at the three angles can be made in quick succession. This last fact reduces greatly the systematic difficulties that arise because of the lapse of time of days between taking data for different angles, unavoidable in the external experiments. The better reliability of the internal data, when they confirm the external data qualitatively, increases confidence in interpretation of the latter.

It should be noted that the collimator is adequate to permit observing neutrons scattered in the external method to be observed with but little background coming through the collimator directly from the lithium target. A considerable background is present, however, as a result of leakage of room scattered neutrons through the sides and back of the shield. The background thus increases rapidly at higher neutron energy.

Table I.

Data on Scattering Samples

Element	Nominal Size	Mass Gm	Average Thickness Inches	Average Diameter Inches	Atoms / Cm^2
C(Graphite)	1/4" x 1-1/2"	11.8615 gm	.2505"	1.4976"	5.234×10^{22}
Iron, Fe (Steel)	1/4" x 1-1/2"	53.944	.2381"	1.4982"	5.115×10^{22}
Cu	1/8" x 1-1/2"	32.363	.1259"	1.4982"	2.697 "
U	1/8" x 1-1/2"	69.689	.1272"	1.5021"	1.542 "
U	1/4" x 1-1/2"	139.194	.2542"	1.5010"	3.086 "
Zr*	Piece A*	15.336	.0815	1.5011	.8869
"	" B	15.369	.0816	1.5006	.8893
"	" C	15.287	.0813	1.5007	.8844

*The notation 2/Zr used in Figs. 2 and 3 means two of these discs were used together as one; 3-Zr that all three were used. The three pieces are so nearly alike that which two of the three were used together makes no difference.

The above samples were used both for the "internal" and "external" experiments.

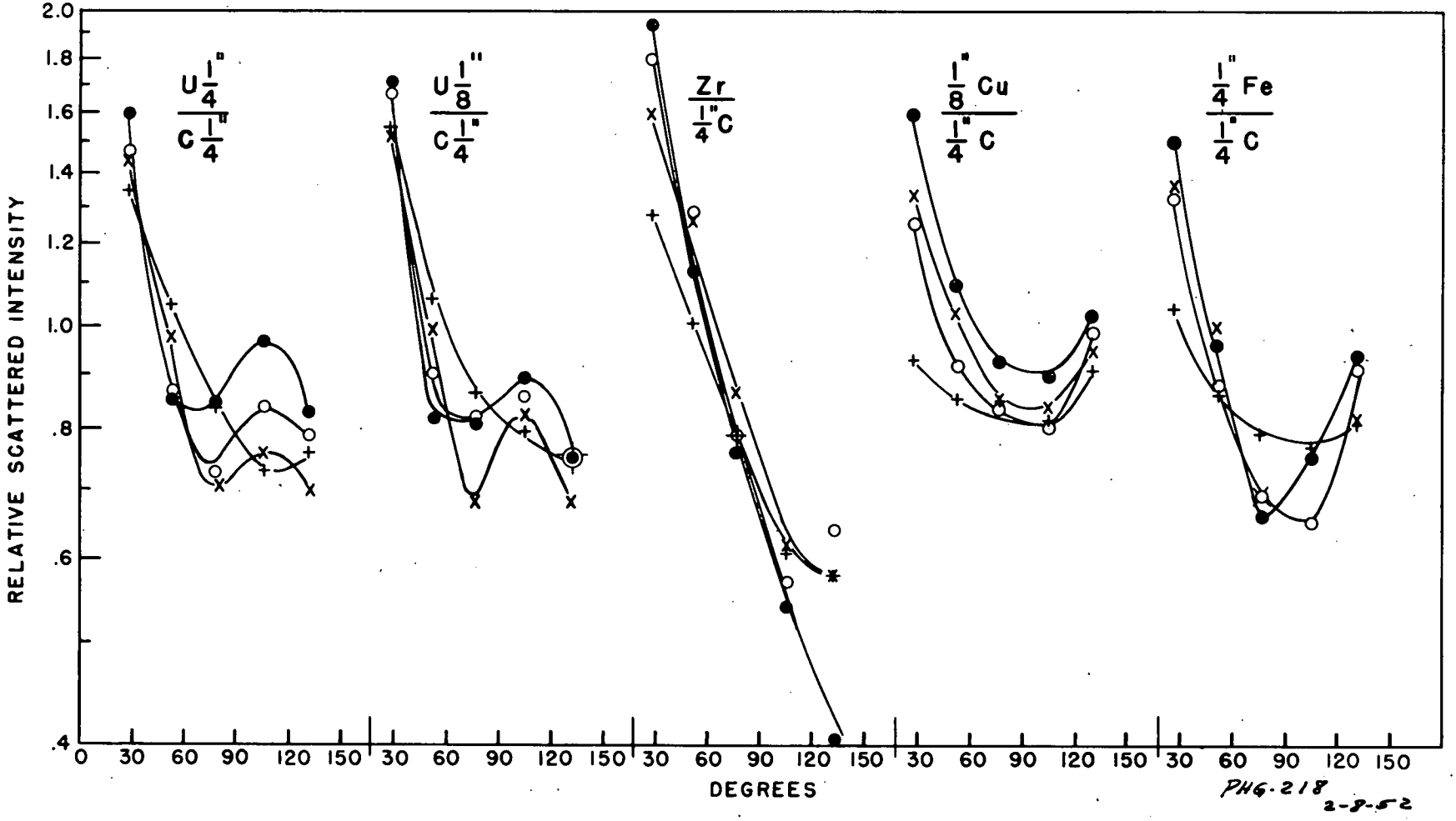

Fig. 2. "External" scattering data.

Plus marks Data at 0.45 Mev neutron energy. Cross Marks X Data at 0.80 Mev neutron energy. Open circles O Data at 1.16 Mev neutron energy. Solid circles ● Data at 1.49 Mev neutron energy. Data on samples in Tables I and II.

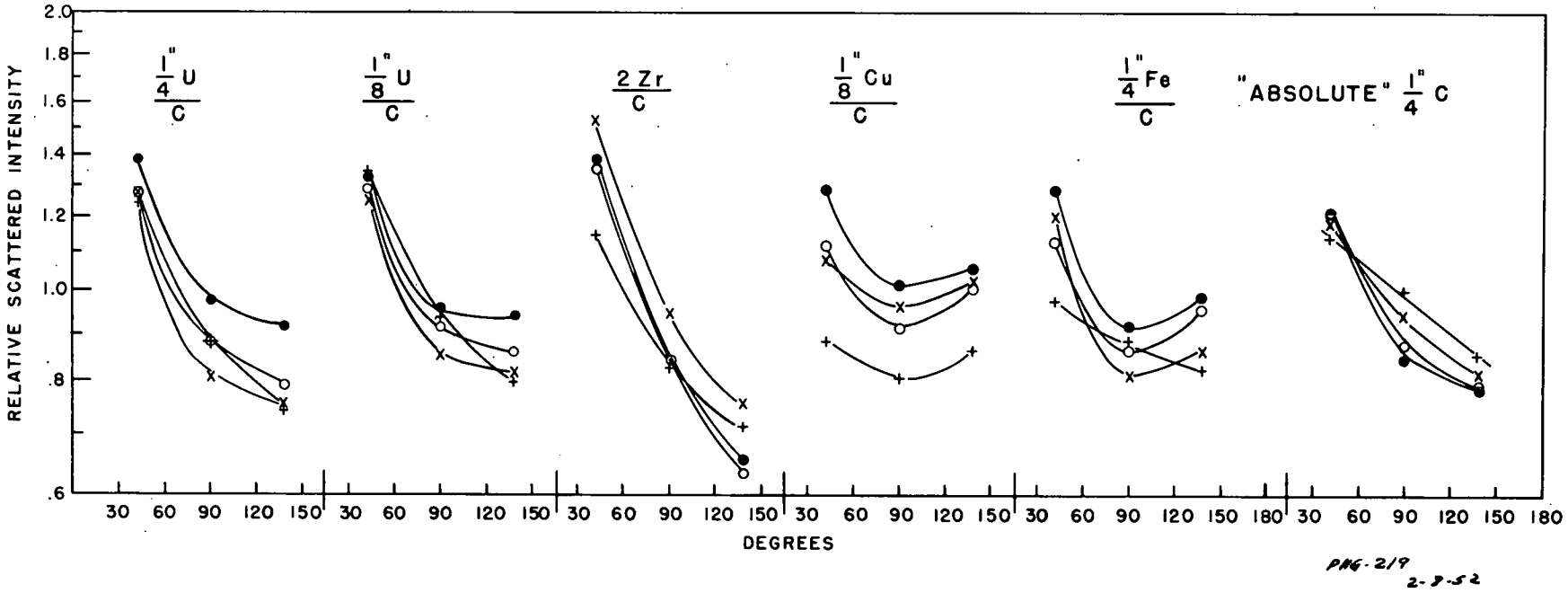

Fig. 3. "Internal" angular distribution data. Same symbols for neutron energies as in Fig. 2. The angle scale has been used arbitrarily so as to make the curves look similar to those of Fig. 2. See text for explanation of "absolute" "1/4" C data. Data on samples in Tables I and II.

Table II.

1. Data on the values of lab angle θ at which measurements were made (external):

$$29.7^{\circ},\ 52.5^{\circ},\ 77.2^{\circ},\ 105.8^{\circ},\ 131.9^{\circ}$$

These are the angles at which the points on the graphs, Fig. 2, are plotted.

2. Orientation of scatterer for "external" geometry:

For the two smallest namely 29.7 and 52.5°, the plane of the disc face of the sample bisected the angle $(180^{\circ} - \theta)$ as shown in Fig. 1. (Called transmission orientation.)

For the remaining three angles, the plane of the sample bisected the angle θ. (Called reflection position.)

3. Note on collimator and viewed region of scatterer (external geometry). The collimator geometry defines a region in front of it from which the detector can receive neutrons. This region has a circular conical shape about one inch in diameter at the scatterer position. This visible part of the scatterer subtends an angle deviating at most about 15° from the central value of θ, and the mean spread in θ is about 10° or a bit less.

Procedure, External Scattering Data.

At each setting of angle, the van de Graaff generator was operated at four settings of the energy. (Electrostatic analyser potentiometer settings of 0.475, 0.55, 0.62, and 0.69 volts) corresponding to 0.45, 0.80, 1.16, and 1.49 Mev neutron energies for Li(p,n) threshold of 1.882 Mev (found at potentiometer setting .4037 to .4046), with target thickness of

approximately 100 kev.

At each energy setting, each scattering sample was in turn placed at the scattering position and readings taken for a fixed amount of integrated beam current. This was the only available method of monitoring the neutron flux to the scattering sample. Serious difficulties were encountered in maintaining the neutron flux proportional to the beam current. This is the subject of the following discussion:

Digression concerning monitoring of neutron flux from lithium target.

A high precision integrator for the beam current was used in this work. It was designed with all known parameters aimed at 0.1% accuracy and appeared in practice to be stable to at least ± 0.2% over a period of many weeks. [Its design is based on charging up to 150 microfarads of condensers with polystyrene dielectric to an accurately determined potential of about 10 volts (periodically checked against a standard cell and adjusting circuit) and letting the beam current discharge the condensers to ground. The ground point is detected by a vibrating diaphragm electrometer and phase sensitive amplifier-detector operating near 400 cycles per second, to trip the counting circuits, etc., at the zero point of charge on the condensers.] It was found, however, that the neutron flux could not be held even to one percent uniformity with respect to this accurate integration of beam current.

The first obvious reason for inability to hold the neutron flux constant was a radial variation in the thickness of the lithium layer. The beam was constrained by a 1/8" wide slit to hit a region on the rotating target of this same width located about 3/4" from the center of rotation of the tantalum cup on which the lithium was deposited. The beam usually focused so that most of it was in a spot about 1/32" to 1/16"

diameter, which spot could wander back and forth over the 1/8" allowable region and still hit the lithium. With the lithium evaporating oven set by trial and error, it was possible to find but not practical to maintain a setting which almost eliminated radial variation in lithium thickness over the required 1/8" strip, to about 1% as judged by the uniformity of the neutron flux.

The next step taken was to insulate the 1/8" wide slit mentioned above and to connect it to ground through a galvanometer. By manually adjusting the beam deflecting magnet and the focus condition it was found that the beam could be held more closely to hitting the lithium always in the same place by keeping this galvanometer reading minimized, i.e., with the beam through the 1/8" aperture quite closely centered.

It was then observed that with the chosen lithium thickness of about 100 kev, only 5 microamperes of beam could be used without burnoff. At 10 microamperes up to 10% of the lithium burned off in several minutes. After this was discovered the beam was held to about 5 microamperes. (A strong air blast did not improve the situation appreciably over using a gentler stream from a small air blower).

After all these steps had been taken, another source of non-uniformity was observed. It was first observed when two neutron monitors were compared. A "long counter" was located straight ahead (at 0° to the direction of the protons), and another smaller paraffin covered BF_3 counter was located overhead (at about 90° to the direction of the proton beam) above the target. For a fixed beam integration cycle, it was noticed that at certain settings for the energy of the beam the counting rate on one of these monitors always <u>increased</u> when the other <u>decreased</u>. Adjustment of the beam analysing magnet to deflect the beam so that it hit the lithium layer at different radii

within the allowed 1/8" region could give this effect reproducibly. The effect was explainable on the basis that as the beam hit the lithium it burned off some lithium in a narrow band and also caused buildup of carbon over the lithium in this narrow band. These presumptions plus the known nature of the yield function of neutrons with respect to angle of emission of the neutrons account for the effect. The perturbation could amount to as much as ten percent, but was held to a smaller value by close attention to beam centering and watching the reproduceability of monitor readings. The problem could not be eliminated, however, since the presence or absence of an external scattering sample in itself changes the readings of both monitoring counters by substantial amounts.

Procedure, external scattering data, continued.

At each setting of angle and energy each scattering sample was in turn placed at the scattering position for a beam integration cycle. This pattern was repeated until each sample had been measured at least twice. The 1/4" C, 1/4" U, and open beam (background) readings were each made four times. The integration cycles were chosen long enough so that the ratio of net counts from a given sample to net counts for carbon had a probable error of not more than about 3 percent for 1/4" U and not over about 7 percent for any other sample except zirconium (see below).

At each energy the direct transmission, T, of each sample was measured and the above scattering ratios corrected by the ratio $t = (1 - T_{sample})/(1 - T_{carbon})$. The data plotted in Fig. 2 are the result of this type of computation. These data indicate very nearly the relative angular variation of scattering of the samples reduced to a basis of equal total cross section. No correction has been made for the error due to using the ratio, t, for normal incidence instead of at the actual

angle of sample at a given scattering angle.

Plotted as shown, the curves for each energy should overlap each other as they do for all but copper. In this case the transmissions were rather large and the error in t seemingly was excessive, causing a systematic shift in the curves vertically in the logarithmic plot used. It is probable that the unexpected large error is due to the same difficulty in monitoring the neutron flux that was discussed above. In the future, the monitoring in transmission measurements should be done with a collimator and detector for the monitoring as well as for the transmission, and with both collimators at equal angles to the forward neutron direction.

The data on 1/4" U and 1/8" U show fair general agreement. The latter data are less accurate, of course. The peak at about 100° appears at 0.8 Mev and becomes more pronounced at high energies.

The data for zirconium show a most pronounced forward scattering with probably no backward increase. The data at 131.9° for Zr are particularly poor. At this angle only two discs were used together and so few counts were obtained that the statistical error in the points is excessive, 10% at 1.16 Mev and 20% at 1.49 Mev. At the other angles, three discs were used so as to obtain more counts, and the statistical errors are 7% at the worst. Copper and iron show both backward and forward peaks, the forward being the larger.

The internal scattering data were treated the same way as the external. Correction by using the above ratio, t, was made using the same value of transmissions, T, as for the external data, with a similar displacement of the curves for copper. There is general agreement of these internal scattering data in Fig. 3 with the data of Fig. 2 for external scattering. Of course there is no sign of the 100° peak in

uranium, except indirectly by the trend toward less asymmetric scattering at high energy, which is opposite to the trend in any other sample.

In Figure 3 the graphs marked "absolute" 1/4 "C" are of questionable significance. They were made from data on graphite by an arbitrary scheme of normalization of internal scattering data which is intended to show that carbon becomes more forward in its scattering as the energy increases. However, a comparison of the data for graphite from this series of experiments and from some earlier ones makes interpretation appear very uncertain. It is clear only that of the materials tested, (1) carbon has much less asymmetric scattering than the others, (2) that at 0.45 Mev carbon is close to symmetric in its scattering (c.m. coordinates), and (3) that its scattering becomes more forward at higher energies (how much cannot be determined quantitatively from the available data).

The difficulties in the interpretation of "absolute" differential cross sections by the internal method include at least the following:

1. The $1\frac{1}{2}$" diameter discs did not intercept the whole beam, there was a fall-off in fraction of beam scattered in going from the forward to the backward position, by an amount not as large as the simple inverse square law would predict, but by an uncertain amount.

2. Neutrons not scattered directly toward the paraffin block are rescattered and detected with (perhaps?) 20% as much efficiency as those directly scattered into the paraffin.

3. Although it is simple to figure the center of mass effect in carbon on the assumption of isotropic scattering in the center of mass system, the weighting to give the counts at each angle is uncertain.

4. The effective geometry of the collimator system is perhaps an unknown function of neutron energy.

5. The counting efficiency of the collimator-detector-paraffin block system is an unknown function of energy.

Final note: How much of the detected angular asymmetry is to be attributed to elastic scattering and how much to inelastic is not determined by any of the above data.

Concerning future work:

The "external" method is too difficult to be worth pursuing in the absence of a satisfactory method of flux monitoring.

The "internal" method is too "fuzzy" to be very useful in its present form.

The most likely approach is to build a very large shielded "room" and use in this "room" a large efficient detector which can be swung around the scatterer to all angles with a fairly good definition of angle. In this way neutron monitoring can be achieved. Before this is done, however, good data must be obtained on the distribution of the energy of neutrons in the beam after passing through the collimator.

Table III

TYPICAL DATA.

Angle, 77° 10', Potentiometer 0.690 (1.49 Mev neutrons), beam about 5 μa .

Integrator

Capacity	Cycles	Scattering Plug	Scattering Sample	M_1 Long Counter	M_2 Small Monitor	Counters Bank 1	Bank 2	Bank 3	Sum Bk 1-2-3	Time in 120ths sec.
150 mfd	1	In	1/4" C	391380	111861	3571	4187	3988	11746	41663
"	"	"	1/4" U	354074	111354	4307	4785	4256	13348	41252
"	"	"	None	441815	11040	2234	3006	3104	8344	41794

Transmission data: Potentiometer 0.690

Integrator

Capacity	Cycles	Scattering Plug	Transmis. Sample						
40 mfd	1	In	1/4" C		33612	36193	49879	47860	133932	
			1/4" U		33099	32452	45187	43503	121142	13655
			None		33248	40416	55402	53646	149464	13597
		Out	None		33249	974	1511	1630	4115	17068

Calculated $T_c = 0.897 \pm .002$, $\sigma_c = 2.07b \pm .05$ $T_u = .808 \pm .002$, $\sigma = 6.92 \pm .08$

II. Group #1 - Reports by C. O. Muehlhause

1. Time-of-Flight Measurements of Neutron Resonances L. M. Bollinger and S. P. Harris

The new one hundred channel analyser has proved to be entirely satisfactory and reliable. Variations in transmission curves greater than expectable statistical variations may be depended upon to indicate true variations in the cross section. In order to effect automatic operation of the equipment the primary requirement is that the analyser be completely reliable over long periods of time. This property has been adequately demonstrated. The second requirement for automatic operation is that proper circuits for safety and for handling unusual contingencies be installed. Simple circuits to perform the following functions are nearly completed and will soon be in operation with the chopper:

a) shutdown if the temperature of the rotor's bearings rises too much

b) shutdown if the oil supply to the bearings fails

c) shutdown if the intensity of the neutron beam is drastically and permanently altered

d) temporary shutdown if the intensity of the neutron beam is drastically but temporarily altered

e) temporary shutdown if the background intensity is drastically but temporarily altered.

Preliminary tests have been made with a flight path of twenty meters that indicate the expected improvement in resolution resulting from doubling the flight path. The two hafnium resonances at ~ 5.7 ev, one in Hf^{177}, the other in Hf^{179}, can be resolved (partially) into two distinct resonances at this increased detection distance. Consideration is being given to a variable flight path, the latter to be accomplished by mounting the detector shed on track and wheels.

Preliminary tests have also been made of the new "methyl borate-phenyl" liquid scintillation counter. Normal boron material was used in an unfavorably shaped container (convex to the beam) in conjunction with imperfect coincidence and analyser circuits. Nevertheless an efficiency of ~10% was indicated for neutrons of ~1000 ev. This is sufficiently encouraging that one might expect an efficiency greater than 50% for:

a) enriched boron material

b) properly shaped detector

c) proper circuitry

This subject is discussed to greater length in section 4.

Resonances in arsenic and normal uranium have been re-examined with the new chopper (cf. ANL-4602, 4552). Table IV lists these results along with those of normal zirconium, U^{233}, and Pu.

Table IV

Material	Thickness Gm/Cm^2	Resonances ev	Comment
As^{75}	6.25	46 ± 2 ~95	
Zr		>5000	cf. sec. 2 for Zr^{91}
U^{233}		1.8, 2.3, 3.5, 4.8, 6.8, 10.5, 13, 17, 22, 120	Major resonances at 1.8, 2.3, 6.8, 10.5
U^{238}	6.0	21.1 ± .8 38 ± 2	
Pu			Same as reported by the Columbia Group

2. Neutron Transmission and Scattering C. T. Hibdon

Various transmission and scattering measurements were made using the annular counter by methods discussed in previous quarterly reports. Table

V lists results on aluminum, iron, nickel, zirconium, and bismuth. The fraction resonance overlap, δ_r, is given along with the transmission cross section at various energies. The value of δ_r naturally depends on the detector width as well as the resonance width and the proximity of the level in the transmitter. No specific energy is given for the vanadium detected cross sections.

Table V

Material	σ	Sub-Cd	Epi-Cd	10.0 ev	19.5 ev	126 ev	345 ev	2300 ev	V
	σ_s								
$_{13}Al^{27}$	σ_t			1.44				1.42	
	δ_r			0				0	
	σ_s								
$_{26}Fe$	σ_t	14.8		11.5	11.0	10.5	9.55	7.08	
	δ_r			0	0	0	0	.14	
	σ_s								
$_{28}Ni^{58}$	σ_t			23.7	23.4	22.5	20.8	19.5	
	δ_r			0	0	0	0	0	
	σ_s	5.58	6.56						
$_{40}Zr$	σ_t			6.25	6.20	6.09	5.84	5.93	5.85
	δ_r			0	0	0	.08	.16	.17
	σ_s	7.55	6.02						
75% Enriched Zr^{91}	σ_t								
	δ_r								

Table V Contin.:

Material	σ	Sub-Cd	Epi-Cd	10.0 ev	19.5 ev	126 ev	345 ev	2300 ev	V
	σ_s								
$_{83}Bi^{209}$	σ_t				9.23				
	δ_r				0				

The presence of a resonance level in zirconium in the kev region is indicated by overlap with manganese, sodium, and vanadium detectors. The fact that the asymptotic transmission cross section is less in this region than at lower energies implies that the resonance energy is greater than 3000 ev. Additional evidence for such a level is given by the data of Shull and Wollan (Phys. Rev. 81, 527, (1951)), namely: $\sigma_{coh} = 4.9$ b. That is, $\sigma_{coh} \neq \sigma_{ths}$ is an indication of a low lying resonance level giving significant scattering.

One would expect Zr^{91} to be the isotope having the lowest lying level since it has the highest thermal capture cross section, and is the only odd isotope in zirconium (magic number plus one). However, the data of Table V indicates this is not the case. In this event $g = 1$, and it is possible, using an additional measurement of self indication ($\sigma_{self} = 21.0$ b), to calculate p, E_o, and Γ on the assumption that $\Gamma_n \simeq \Gamma$. Such a calculation would be unreliable, however, because both the peak cross section and the resonance scattering integral are too sensitive to the small fraction of resonance scattering: $\sigma_{epi-Cd} - \sigma_p / \sigma_{epi-Cd}$.

3. Internal Conversion of Capture γ-rays. C. T. Hibdon

Further measurements on the prompt internal conversion electrons emitted on neutron capture were carried out using a permanent 103 gauss magnet. Various K, L, and M lines were observed indicating γ-rays of 85.3, 107.9 and 193.7 kev, the latter being the crossover γ-ray of the first two.

Intensity measurements of the 89 kev γ-ray[1] from 2.6 hour Dy^{165} indicate that this γ-ray is ten to one hundred times weaker than the 85 kev prompt γ-ray. The 89 kev γ-ray (of Ho^{165}) is, therefore, different from and distinguished from the prompt 85 kev capture gamma ray of Dy^{165}.

1. R. A. Caldwell, Phys. Rev. 78, 407, (1950).

4. Liquid Scintillation Counters C. O. Muehlhause and G. E. Thomas

a) Slow Neutron Counters

Further investigation of liquid scintillation counters for neutrons made with methyl borate-terphenyl-in-phenylcyclohexane mixtures has been carried out. The pulse height distribution has been compared with that resulting from a 0-16 kev electron band, and also with a 16 kev electron group. Both comparisons indicate that the boron disintegration pulse height distribution is peaked at about 40 kev equivalent electron energy, and has a width at half maximum of about 100 kev, and is essentially zero at about 150 kev. Further measurements of this sort will be undertaken by introducing suitable radioactive materials into the detecting medium.

Tube noise starts at about 5 kev. In order to effect measurements of the type described, a photomultiplier tube system capable of being cooled by either dry ice and acetone or by liquid air was constructed out of pyrex glass. The photo tube and light pipe were sealed in pyrex tubes having ground glass joints. The 5819 leads were brought through sealed glass connections to the resistor bank and cathode follower. This was done to prevent cooling of the electrical parts with consequent deposition of water and ice on the sensitive components of the circuitry.

A counter of a volume of only one cubic millimeter was constructed for detection of thermal neutrons only. Such a counter allows study of pulse heights with negligible interference from γ-rays. The present model, however, contains a conical lucite light pipe having a volume over ten thousand times greater than that of the neutron-sensitive liquid. The γ-ray sensitivity of the lucite made this counter impractical near a pile beam. An improved model having no such large lucite mass is being made.

Both experiment and calculation show that the efficiency of the liquid scintillating medium for detection of γ-rays is $\sim$2% for one gram/cm^2 and

typical γ-rays (e.g. band from 150 to 1500 kev) in the bias range from 0 to 150 kev. The brief mention of this matter in the previous quarterly report ANL-4746, p. 27, should have referred to the biasing out of electrons rather than of γ-rays of a given energy. This is so because electrons are generated by γ-rays in the organic medium primarily via the Compton effect. Low energy γ-rays result in electron recoils of energies considerably lower than those of the γ-rays themselves.

An interesting theoretical aspect of the inert property of boron esters in a liquid scintillation medium is that their introduction into such a medium allows one to distinguish the reaction parameter involving transmission and trapping of energy originally in the solvent from the reaction parameter involving emission and quenching by the solute. After the method of Kallmann,[1,2] a brief derivation will now be given for the variation of pulse height, h, with concentration, c_f, of fluorescent material, f; concentration, c_s, of proper solvent material, s; and dilution factor, n, of an inert material. Such a three-component system is illustrated by identifying f with terphenyl, "s" with phenylcyclohexane, and the inert material with methyl borate.

Assume that the passage of ionizing radiation excites a certain number of molecules in "s" into states such that the energy may be transferred to "f", but that no such states may be excited in the inert material. Let n_e, be the number of "s"-states per unit concentration of "s". The energy in the $n_e c_s$ states is now either quenched in or by s, or transferred and trapped in "f". Thereafter it is either quenched in or by "f", or emitted as light from "f". Let the probabilities per unit time $1/\tau$, for these various processes be defined as follows:

1. H. Kallmann, M. Furst, Phys. Rev. 79, 857 (1950).
2. H. Kallmann, Third Quarterly Report, New York University, U. S. Signal Corps Contract No. 36-039 sc-5487.

$1/\tau_{is}$ = internal quenching in "s"

$1/\tau_{gs}$ = self quenching by "s"

$1/\tau_{tf}$ = transfer and trapping in "f"

$1/\tau_{if}$ = internal quenching in "f"

$1/\tau_{gf}$ = self quenching by "f"

$1/\tau_{ef}$ = emission from "f"

The two types of quenching, internal and self, are two modes of decay: the first being independent of concentration, and the second being proportional to concentration.

$$1/\tau_{tf} = \alpha c_f \qquad 1/\tau_{gs} = \beta c_s \qquad 1/\tau_{gf} = \gamma c_f$$

where α, β, and γ are constants.

$$h = n_e c_s \frac{1/\tau_{tf}}{1/\tau_{tf} + 1/\tau_{gs} + 1/\tau_{is}} \cdot \frac{1/\tau_{ef}}{1/\tau_{ef} + 1/\tau_{gf} + 1/\tau_{if}}$$

$$h = n_e c_s \frac{\alpha c_f}{\alpha c_f + \beta c_s + 1/\tau_{is}} \cdot \frac{1}{\gamma \tau_{ef} c_f + 1 + \tau_{ef}/\tau_{if}}$$

$$h = \frac{n_e c_s}{\gamma \tau_{ef}} \cdot \frac{c_f}{\left[c_f + 1/\alpha (\beta c_s + 1/\tau_{is})\right] \left[c_f + 1/\gamma (1/\tau_{ef} + 1/\tau_{if})\right]}$$

Or in Kallmann's notation let:

$$P = \frac{n_e c_s}{\gamma \tau_{ef}} \qquad Q = 1/\alpha \ (\beta c_s + 1/\tau_{is}) \qquad R = 1/\gamma (1/\tau_{ef} + 1/\tau_{if})$$

$$c_f = c \text{ and } h = \frac{Pc}{(Q + c)(R + c)}$$

Let the subscript "0" indicate parametric values for the case of no inert material. Then:

$$P_o = \frac{n_e c_{so}}{\gamma \tau_{ef}} \qquad Q_o = 1/\alpha (\beta c_{so} + 1/\tau_{is}) \qquad R_o = 1/\gamma (1/\tau_{ef} + 1/\tau_{if})$$

$$P = P_o \, c_s/c_{so} \qquad Q = Q_o \frac{\frac{c_s}{c_{so}} + \frac{1}{\beta \tau_{is} c_{so}}}{1 + \frac{1}{\beta \tau_{is} c_{so}}} \qquad R = R_o$$

$c_{fo} = c_o$, and if $c = nc_o$, then $c_s \simeq nc_{so}$

Let $\delta = 1/\beta \tau_{is} c_{so}$ then, by substitution

$$h = \frac{n^2 P_o c_o}{\left(Q_o \frac{n+\delta}{1+\delta} + nc_o\right)(R_o + nc_o)}$$

$$= \frac{nP_o c_o}{\left(Q_o \frac{1+\delta/n}{1+\delta} + c_o\right)(R_o + nc_o)}$$

If the internal quenching of the solvent molecules is considerably less than the self-quenching by other molecules of the solvent ($\tau_{is} >> \tau_{gs}$) $\delta << 1$ and the above expression reduces to the simpler one:

$$h = \frac{nP_o c_o}{(Q_o + c_o)(R_o + nc_o)}$$

which for $n = 1$ is the same as Kallmann's expression. From the study of various mixtures Kallmann arrived at values of 1.1 gm /ℓ and 100 gm/ℓ for the constants Q_o and R_o. Because of the symmetry of the expression with $n = 1$, however, it was not possible to be certain as to which numerical value was to be associated with either particular theoretical constant, Q_o or R_o. The use of the diluent makes it possible to make this distinction. It was found experimentally that upon dilution "h" decreases in proportion to "n", which would be found only for $R_o >> c_o$ and $\delta << 1$. Since in the dilution experiments c_o had values ~ 3 gm /ℓ R_o must correspond to the constant, 100 gm/ℓ, rather than to the other constant, 1.1 gm/ℓ.

The maximum pulse height from the above expression is obtained for a concentration, $c = \sqrt{nQ_oR_o} = 7.4$ gm/ℓ for $n = 1/2$, and 10.5 gm/ℓ for $n = 1$. At room temperature the solubility of terphenyl in phenylcyclohexane is ~ 3.5 gm/ℓ ($n = 1$). In the diluted material ($n = 0.5$) the solubility of terphenyl is somewhat higher, and the optimum concentration is more readily approached. It is desirable in either case to saturate the solution for alpha detection (i.e. boron disintegration). At slightly higher temperatures the optimum concentration of terphenyl as determined by room temperature parameters is readily obtained. However, there may be greater advantage in

working at lower temperatures if by so doing the various quenching probabilities are reduced.

The presence of the fourth component diphenyl hexatriene further complicates the situation and has not been analyzed carefully to date. The probable experimental procedure would be to slowly add diphenyl-hexatriene to a saturated solution of terphenyl until the pulse height observed is a maximum. This amount is ~7 mg/ℓ.

b) γ-Ray Counters

Several attempts to make scintillation counters of tetraethyl lead and terphenyl-phenylcyclohexane failed. The medium fluoresced well under an ultra violet lamp, but gave pulse heights only ~2% of those from anthracene. It is hoped that the mercury alkyls, being more stable, will not quench the fluorescence.

If a mercury containing medium were successful it would also make an interesting neutron counter; the high thermal capture cross section of mercury would make such counters rather efficient for neutrons, and also result in enormous pulse sizes (~7 Mev) via its extreme sensitivity to its own capture γ-rays. Such a counter would, however, possess an uncertain detection time ~4μs (~2μs age plus ~2 μs thermal). This is to be contrasted with the neutron lifetime in the methyl borate phenyl counter of ~0.4 μs.

One attempt was made to introduce ethyl iodide into a terphenyl solution without success. Pulse heights were only ~3% of those from anthracene. Again, other organo-iodine compounds such as methylene iodide may be successful. The analogous bromine compound, ethyl bromide likewise quenched the terphenyl fluorescence when the former was present in sufficiently large quantities.

III. Studies with the Scintillation Gamma Ray Spectrometer. Bernard Hamermesh and Virginia Hummel.

1. Sc^{46} (20 sec).

The energy of the gamma ray from the 20 second isomer of Sc^{46} has been determined as 142 ± 5 Kev. This was done since there had been some conflicting reports as to the value of the energy as determined by an internal conversion spectrometer and by a scintillation counter. All methods are now in agreement.

2. The Gamma Ray from the First Excited State of Li^7.

As a check on the reliability of the instrument, a measurement of the gamma ray from the first excited state of Li^7 was made. The beam of neutrons from hole #7 at CP3 was scattered onto a boron sample and the gamma rays were observed. The annihilation radiation that arises from the scattered pile gamma rays striking the bismuth jaws of the slit system was used to calibrate the instrument. The energy was determined as 485 ± 5 Kev.

3. Thermal Neutron Capture Gamma Rays.

The program of studying the capture gamma ray spectra of the elements of atomic numbers 19-30 (K - Zn) is continuing. Work on Sc, Cr, Mn and Fe has been reported previously (ANL-4746 and (ANL-4680). Nickel and copper have now been studied. In addition, work has begun on cobalt, zinc and titanium. The program was interrupted to study the gold spectrum since this is of particular interest to our "hot atom" chemists.

Copper.

There appears to be lines in the region between 6.5 and 8.0 Mev. The resolution of the instrument is too poor to resolve any of these lines. In the low energy region there is one very intense line at 150 ± 10 Kev.

Nickel.

The spectrum has many unresolved lines in it. There is no evidence of any low energy lines. But there is evidence of many lines between 6.5 and 7.5 Mev and between 8.5 and 9.5 Mev. The spectrum seems to be very complex.

Gold.

The gold spectrum in the low energy region shows a line at 70 Kev. This is probably the K x-ray. A line at 410 Kev is observed which remains when the neutron beam is shut off. This line is the line associated with the beta decay of Au^{198}. There are many high energy lines but only one stands out sufficiently so as to be resolved. This line is at 6.2 Mev.

IV. Flux Measurements in the EBR (P. J. Persiani* and G. R. Ringo)

The EBR is a fast neutron reactor with a core of U^{235} surrounded by a blanket of natural U, surrounded in turn by a graphite reflector. In order to measure the flux in this reactor phosphorous foils were irradiated and the 2.7 hr activity from the Si^{31} produced by the n-p reaction was counted. This reaction has a threshold near 1 Mev so the activity is mainly caused by unmoderated fission neutrons. The foils were calibrated by placing them in a known fission neutron flux from a plate of U^{235} exposed to the flux from the thermal column of the EBR. As a measure of the moderated part of the spectrum, gold foils were used.

As would be expected, the ratio of gold to Si activity increases greatly in going from the core to the reflector. The Si activity indicated that there is a flux of 1.3×10^{14} fission neutrons/cm^2 sec in the center of the core at 1000 Kw power and a flux of 6×10^6 20" outside the end of a 2" diameter collimator that goes to the blanket. From this collimator, of course, there is a considerable flux of slower neutrons also (although, in the present arrangement no more in the resonance region than would come from a comparable hole in CP-3). The thermal flux from the thermal column appears to be twice that of CP-3' i. e. 9×10^7. More detailed results of these flux measurements will be presented in a report of the Reactor Engineering and Services Division.

---

*Reactor Engineering and Services Division.

V. Xenon Content of the Atmosphere. (R. J. Hayden & D. G. Karraker)

The xenon content of the atmosphere was measured by the mass spectrometric isotopic dilution method using techniques similar to those previously used for the krypton content (ANL-4602). Briefly, standard Xe^{128} tracers were produced by neutron irradiation of sodium iodide. The xenon so obtained was introduced at constant pressure into a number of sample tubes of known volume. The Xe^{128} content of several of these volumes was measured by diluting them against measured quantities of spectroscopically pure xenon. This procedure served to give the pressure and hence the total quantity of Xe^{128} in each of the remaining sample tubes. Certain of these remaining sample tubes were mixed with measured quantities of air. After isotopic mixing had been assured, the xenon was extracted by a standard gas purification train. Mass spectrometric analysis of this xenon served to determine the absolute amount of xenon present in the known quantity of air. The ratio of these figures gave the relative abundance of xenon as compared to dry air. The average of three determinations showed xenon to be present to 0.109 ppm by pressure. At present this figure is believed good to 5%. Further calibration is expected to increase the precision of the result by approximately a factor of two.

Previous results have given values of 0.09 ppm[1], 0.04 ppm[2], and 0.09 ppm[3], for this quantity.

---

(1) Damkohler, G., Z. Elektrochem 41, 74 (1935).
(2) Goldschmidt, V. M., Skrifter Norske Videnskap-Akad., Oslo. I. Mat.-Naturv. Klasse No. 4 (1937).
(3) Paneth, F. A., Quart. J. Roy. Meteorol. Soc. 65, 303 (1939).

VI. Neutron Diffraction Investigation of the Atomic Magnetic Moment Orientation in the Antiferromagnetic Compound CrSb. A. I. Snow*

The atomic magnetic moment orientation in the antiferromagnetic compound CrSb has been investigated at room temperature by neutron diffraction. The crystal structure and magnetic properties of this compound have been previously determined by Haraldsen, Rosenqvist and Gronvold.[1] This compound has the nickel arsenide structure and shows a marked decrease in magnetic susceptibility as the temperature is lowered from the antiferromagnetic Curie point (450° C.). The magnetic mass susceptibility falls from 10.97×10^{-6} at 450° C. to 3.3×10^{-6} at 20° C. Lattice constants are $a_o = 4.127$ A and $c_o = 5.451$ A.

Calculation showed that all antiferromagnetic magnetic moment orientations which lead to a magnetic unit cell, one side of which is a multiple of the atomic (X-ray) unit cell, would cause the presence of strong new diffraction maxima at low angles in a neutron diffraction pattern. Such new maxima were not observed, though carefully looked for. Experimental data showed that the (101) maximum had twice the intensity of the (102) and (110) maxima, respectively. On the basis of nuclear scattering, with no magnetic scattering, these three maxima would be essentially equal in magnitude. This doubling in intensity of (101) relative to (102) and (110), respectively, is consistent with the atomic magnetic moments being aligned perpendicular to (001) planes, i. e., along the c axis, in such a manner that they are aligned in the same direction (ferromagnetically) in any one (001) plane but oppositely directed (antiferromagnetically) in adjacent (001) planes. Nearest neighbor chromium atoms (2.726 A apart) are thus aligned antiferromagnetically whereas second nearest neighbors (4.127 A apart) are aligned ferromagnetically. One unit

*Institute for the Study of Metals, University of Chicago, Chicago, Illinois.

1. H. Haraldsen, T. Rosenqvist and F. Gronvold, Archiv for Mathematik Naturvidenskab. B. L. Nr. 4.

cell is shown in Figure 4. The possibility that the magnetic moments may be aligned parallel to the (001) planes may be eliminated since this arrangement would lead to an unobserved strong maximum at low angles.

On the basis of the relative intensity data, a conservative estimate for the average number of electrons per atom whose magnetic moments are aligned in the manner described above is 2.7 ± 0.2, if the assumption is made that the orbital angular momentum contribution is completely quenched and the magnetic amplitude form factor of manganese[2] is used in the calculation.

The atomic magnetic moment orientation found above differs from that found in MnF_2 which is body centered tetragonal with respect to the manganese atoms, where nearest neighbors (3.31 A apart)[3] are ferromagnetically arranged and next nearest neighbors (3.82 A apart)[3] are antiferromagnetically arranged.[4] The CrSb arrangement is somewhat similar to the arrangement in some of the (111) planes of the face centered cubic compound FeO[2] since in FeO the moments are aligned perpendicular to some of the (111) planes and are aligned in opposite directions in adjacent (111) planes[4] of the particular sets considered.

Thanks are due to Dr. T. Rosenqvist for preparation of the compound. The neutron diffration work was performed by the author at the spectrometer at CP-3'.

2. C. G. Shull, W. A. Strauser and E. O. Wollan, Phys. Rev. 83, 333 (1951).
3. Calculated from lattice constants of M. Griffel and J. W. Stout, J. Am. Chem. Soc. 72, 4351 (1950).
4. Discussed by C. G. Shull at the Pittsburgh meeting of the American Physical Society on March 10, 1951.

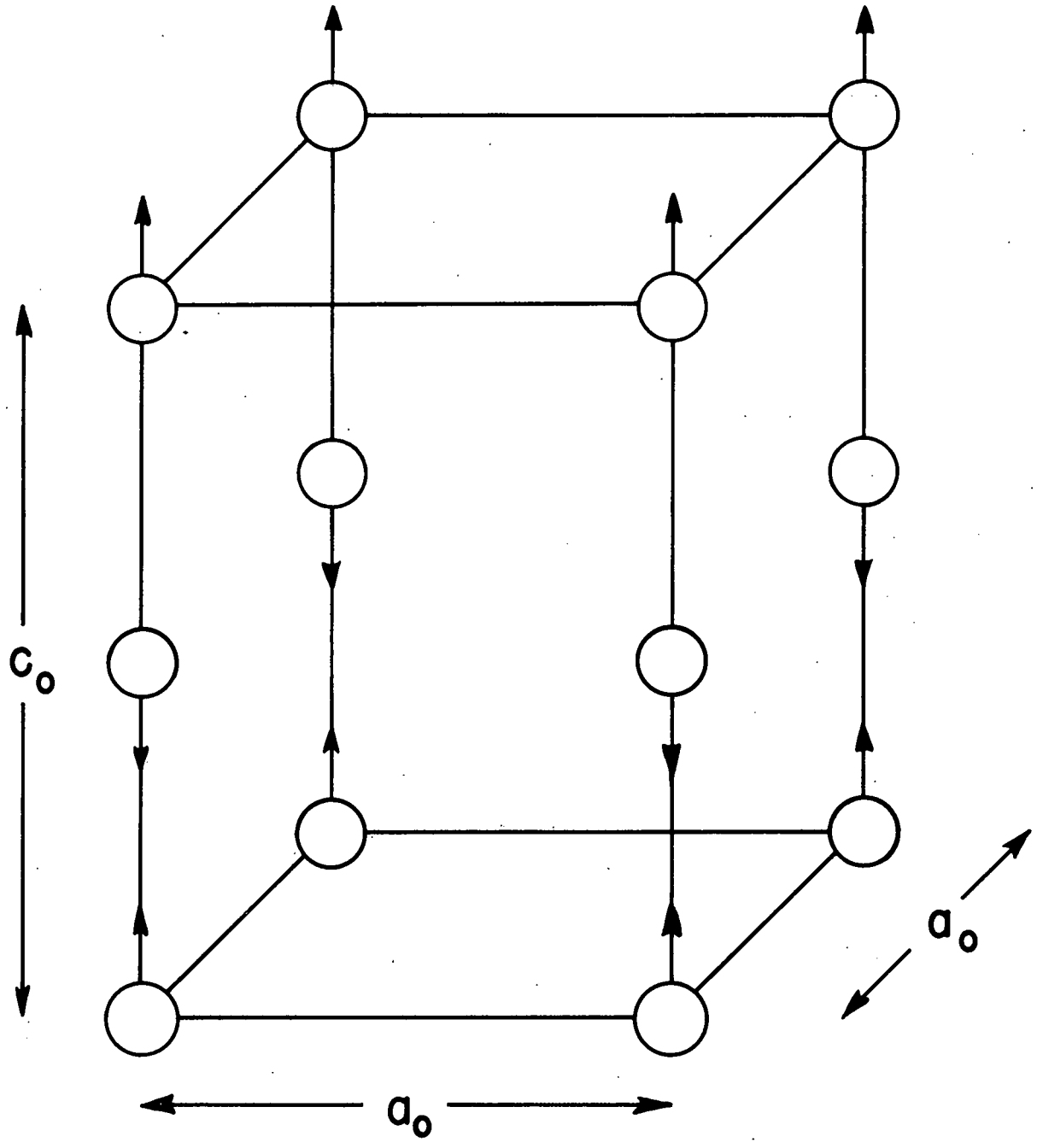

PHG-281
4-14-52

Unit Cell of CrSb

Fig. 4

VII. Crystallography - Reports by W. H. Zachariasen

1. The Crystal Structure of Neptunium Metal (W. H. Zachariasen, H. A. Plettinger)

Attempts to interpret the x-ray powder photograph have finally succeeded.

The metal is orthorhombic with the following dimensions of the unit cell[1)]

$a_1 = 4.722 \pm 0.002$ Å, $a_2 = 4.894 \pm 0.003$ Å, $a_3 = 6.666 \pm 0.003$ Å.

These values are in Å rather than kX units. Using an atomic weight of 237.0 the calculated density with eight neptunium atoms per unit cell is $\rho = 20.42 \pm 0.04$ gcm^{-3} at room temperature.

The space group is Pmcn (D_{2h}^{16}), and the atomic positions are:

4 atoms Np(I) in $\pm (\frac{1}{4}, y_1, z_1)(\frac{1}{4}, \frac{1}{2}-y_1, z_1+\frac{1}{2})$

4 atoms Np(II) in $\pm (\frac{1}{4}, y_2, z_2)(\frac{1}{4}, \frac{1}{2}-y_2, z_2+\frac{1}{2})$

The best parameter values are[1)]

$y_1 = 0.208 \pm 0.005$ $\quad z_1 = 0.036 \pm 0.005$

$y_2 = 0.158 \pm 0.005$ $\quad z_2 = 0.319 \pm 0.005$

Each neptunium atom has four close neighbors at 2.60 Å, 2.63 Å, 2.64 Å, 2.64 Å, a fifth neighbor at 3.05 Å. A neptunium atom of the first kind, Np(I), has eleven neighbor atoms in the range 2.60 Å to 3.35 Å, while a Np(II) atom has thirteen neighbor atoms in the range 2.60 Å to 3.53 Å. The smallest angles between the bonds to the four nearest atoms are $84\frac{1}{2}^\circ$ and $89\frac{1}{2}^\circ$ for Np(I), 79° and 89° for Np(II).

---

1) These values have been obtained from new diffraction patterns and supercede those given in the memorandum ANL-FWHZ-199.

In alpha uranium there are also four close neighbors, the smallest bond angles being 90°.

2. Anomalous Transparency of Thick Crystals to X-Rays (W. H. Zachariasen, H. A. Plettinger)

G. Borrmann[1] has observed that some crystal specimens are considerably more transparent to x-rays when the incident beam produces diffraction than one calculates from the usual absorption law. The effect is quite striking as illustrated by Borrmann's observation on a particular calcite crystal in which the transmitted beam has an intensity 10^{19} times greater than calculated from the ordinary absorption coefficient. Similar observations were later reported by H. N. Campbell.[2]

The effect can be quantitatively explained by means of the dynamical theory of x-ray diffraction for thick, absorbing crystals.[3] The effective absorption coefficients as measured by Borrmann and Campbell are in excellent agreement with the values deduced from theory. For $\lambda = 1.54$ Å the usual linear absorption coefficient of calcite is $\mu_0 = 193\ cm^{-1}$. The observed and calculated values in the region of anomalous transparency are

Crystal thickness	Observed	Calculated
0.212 cm	30.2 cm^{-1}	30.5 cm^{-1}
0.271 cm	27.7 cm^{-1}	28.6 cm^{-1}

An account of the investigation is given in a forthcoming special report.

A similar effect may be expected in neutron diffraction.

---

1) G. Borrmann, Phys. Z. 42, 157 (1941); Z. f. Phys. 127, 297 (1950).
2) H. N. Campbell, J. Appl. Phys. 22, 1139 (1951).
3) W. H. Zachariasen, "Theory of X-Ray Diffraction in Crystals", 1945.

3. The Crystal Structure of Neptunium Carbides (W. H. Zachariasen, H. A. Plettinger)

In samples of neptunium carbides prepared by Sherman Fried three phases have been identified: NpC, Np_2C_3 and NpC_2.

NpC

This phase was found as a minor constituent in a sample consisting primarily of Np_2C_3.

NpC has the sodium chloride type of structure with

$$a = 5.003 \pm 0.003 \text{ Å}.$$

Np_2C_3

The sesqui carbide is cubic and isostructural with Pu_2C_3 previously reported.

The unit cell constant is

$$a = 8.1036 \pm 0.0005 \text{ Å}.$$

NpC_2

The dicarbide is isostructural with the analogous thorium and uranium carbides, the structures of which have been described by Hunt and Rundle.[1)]

The tetragonal pseudo-cell (the symmetry is truly monoclinic) has dimensions

$$a_1 = 3.580 \pm 0.005 \text{ Å} \qquad a_3 = 6.030 \pm 0.005 \text{ Å}.$$

1) E. B. Hunt and R. E. Rundle, JACS. (In press).

4. The Crystal Structure of Monoclinic HBO_2

The crystal structure of monoclinic HBO_2 was reported in the Quarterly Report ANL-4659, p.65.

Refinements in the 27 parameter values are being made by the method of successive approximations so that precision values for the interatomic

distances can be obtained. A second approximation has been carried out and a third approximation is in progress.

In the second approximation the interatomic distances are:

$B_I - O_I$	1.33 Å	$B_{III} - O_I$	1.43 Å
$B_I - O_{II}$	1.38	$B_{III} - O_{II}$	1.45
$B_I - O_{III}$	1.37	$B_{III} - O_{IV}$	1.45
$B_{II} - O_{III}$	1.37	$B_{III} - O_{VI}$	1.56
$B_{II} - O_{IV}$	1.37	$O_{II} - H - O_{VI}$	2.70
$B_{II} - O_V$	1.32	$O_{IV} - H - O_V$	2.68
		$O_V - H - O_{VI}$	2.68

It is hoped that the third approximation will yield also the hydrogen positions.

5. The Crystal Structure of Orthoboric Acid, H_3BO_3 (W. H. Zachariasen, H. A. Plettinger)

The approximate crystal structure of H_3BO_3 was reported in 1934.[1] A precision determination of the boron and oxygen positions has been made with the aid of intensity measurements with a Geiger counter. Direct determination of the hydrogen positions are under way.

The results available at present are given below.

The dimensions of the triclinic unit cell containing four molecules are:

$a_1 = 7.039$ Å, $a_2 = 7.053$ Å, $a_3 = 6.578$ Å

$\alpha_1 = 92°35'$, $\alpha_2 = 101°10'$, $\alpha_3 = 119°50'$

1) W. H. Zachariasen, Z.f. Krist. 88, 150-161 (1934).

The 24 parameters for boron and oxygen atoms are:

	x	y	z
B_I	0.647	0.426	0.250
B_{II}	0.312	0.759	0.250
O_I	0.425	0.302	0.250
O_{II}	0.770	0.325	0.250
O_{III}	0.741	0.646	0.250
O_{IV}	0.531	0.882	0.250
O_V	0.211	0.537	0.250
O_{VI}	0.181	0.851	0.250

O - O distances in the BO_3-groups lie in the range 2.32 - 2.37. The O - H - O distances are 2.68 - 2.76 Å.

The differences from the 1934 structure are minor.

VIII. Natural Uranium - H_2O Lattice Calculation - D. Kurath

The following results were obtained from the theoretical treatment of a one-dimensional lattice consisting of plates of natural uranium of thickness, t, coated with ten mils (0.025 cm) of aluminum and separated by a water gap of thickness w. The fast fission factor, ϵ, the probability of resonance escape, p, the thermal utilization factor, f, and the multiplication constant $k = \eta \epsilon p f$ are given in the following table. They are listed as functions of uranium concentration, $\frac{U}{U+H_2O} = \frac{t}{t+w}$, for three values of t.

	$\frac{U}{H_2O+U}$	ϵ	p	f	$k=1.315\ \epsilon\ p\ f$
t=0.50 cm	0.60	1.12	.537	0.951	0.751
	0.50	1.10	.647	0.935	0.874
	0.33	1.065	.798	0.882	0.985
	0.25	1.05	.861	0.829	0.986
t=1.00 cm	0.60	1.12	.594	.950	0.831
	0.50	1.10	.701	.927	0.940
	0.33	1.065	.834	.856	1.000
	0.25	1.05	.886	.782	0.957
t=1.50 cm	0.60	1.12	.621	.943	0.863
	0.50	1.10	.723	.914	0.956
	0.33	1.065	.849	.817	0.972
	0.25	1.05	.898	.716	0.888

The optimum values are:

t	Conc.	k
0.50	0.28	0.99
1.00	0.33	1.00
1.50	0.38	0.99

Calculation of ϵ

For neutrons above the U^{238} fission threshold ($\sim$ 1.5 Mev) the mean free path is greater than the dimensions of the system, so the medium was considered to be homogeneous. The distribution in energy of the flux,

resulting from impressing a fission spectrum on the medium, was obtained from solution of the slowing-down integral equation by iteration. The resulting flux was used to calculate ϵ. Constants used were:

$$(\sigma_s)_H = 6.8\ E\ (e^{-0.85\ E} + 0.05\ e^{-0.14\ E})\ \text{barns} \qquad (E \geq 1.5\ \text{Mev})$$

$$(\sigma_s)_O = 2.0\ E\ (e^{-0.42\ E})\ \text{barns} \qquad (E \geq 1.5\ \text{Mev})$$

$$(\sigma_{fiss})_U = \begin{cases} 0 & E < 1.5\ \text{Mev} \\ 0.364 + 0.053\ E\ \text{barns} & E \geq 1.5\ \text{Mev} \end{cases}$$

$$(\sigma_{in})_U = 4\ (\sigma_{fiss})_U \qquad \nu_U = 2.50$$

The fission spectrum, normalized to unity, can be represented by $f(E) = 0.484 \sinh \sqrt{2E}\ e^{-E}$ (ref. Watt, LA-718). This was approximated by:

$$f(E) = \begin{cases} 0.73\ e^{-0.56\ E} & \text{for } 1.5 \leq E \leq 5\ \text{Mev} \\ 1.92\ e^{-0.77\ E} & \text{for } E \geq 5\ \text{Mev} \end{cases}$$

Calculation of p

The uranium capture cross section was used in the form obtained from the resonance integral:

$$\ln\left(\frac{E_1}{E_o}\right)(\sigma_a)_U = \int \sigma_a \frac{dE}{E} = A\left[1 + \frac{B}{C + \frac{\text{Mass}}{\text{Surface}}}\right]$$

Inserting the constants used gives:

$$(N\sigma_a)_U = \frac{N_U}{5.6}\left[8.5\left(1 + \frac{2.82}{0.1 + 9.45\ t}\right)\right] \quad \text{barns}$$

The scattering cross section used for water was:

$$(N\sigma_s)_{H_2O} = 1.35\ \text{cm}^{-1}$$

These cross sections were modified by disadvantage factors obtained from a one-group, two-region diffusion calculation. They were also multiplied by concentration factors so that the effective cross sections were:

$$(N\sigma_a)_{eff} = \left(\frac{t}{t+w}\right)(d_U)\ (N\sigma_a)_U$$

$$(N\sigma_s)_{eff} = \left(\frac{w}{t+w}\right)(d_w)\ (N\sigma_s)_{H_2O}$$

Then the resonance escape probability is given by:

$$p = \exp\left[\frac{-5.6(N\sigma_a)_{eff}}{(N\sigma_a)_{eff} + (N\sigma_s)_{eff}}\right] \text{ where } 5.6 = \ln\left(\frac{E_1}{E_o}\right)$$

Calculation of f

The thermal utilization is obtained from solving the diffusion problem for thermal neutrons in the system, giving the formula:

$$\frac{1}{f} = \left(\frac{w}{2}\right)(N\sigma_s)_w \left[\left\{\frac{\coth\left(\frac{K_w w}{2}\right)}{D_w K_w} + \frac{\coth\left(\frac{K_U t}{2}\right)}{D_U K_U}\right\} \cosh K_A \Delta + \left\{1 + (D_A K_A)^2 \left(\frac{\coth\left(\frac{K_w w}{2}\right)}{D_w K_w}\right)\left(\frac{\coth\left(\frac{K_U t}{2}\right)}{D_U K_U}\right)\right\} \frac{\sinh K_A \Delta}{D_A K_A}\right]$$

where the subscripts w, U, A refer to water, uranium and aluminum with thicknesses w, t, Δ respectively. The constants used were:

	Water	Uranium	Aluminum
K	0.350	0.769	0.056
D	0.142	0.522	4.00
DK	0.0497	0.401	0.226
$N\sigma_s = DK^2$	0.0175	0.309	0.0128

IX. Zero Power Reactors for Research Purposes (B. I. Spinrad, D. Kurath, H. K. Clark

An investigation of properties of reflected water-boiler reactors has been made for the purpose of determining feasible systems for use as low level neutron sources.

We have calculated the critical properties of spherical systems in which the core is H_2O-U^{235}, and the reflector is BeO, Graphite, or a mixture. The following tables summarize the results:

TABLE VI - Critical Properties of U^{235}-H_2O Solutions with Infinite Graphite Reflector.

	Core Radius (cm)	Core Concentration (g/liter)	K core	M(grams)
	16.0	34.3	1.5	588
	14.25	43.7	1.6	530
	13.45	50.1	1.65	510
Minimum	12.7	58.3	1.7	500
Mass	12.1	68.6	1.75	508
	11.5	82.1	1.8	523
	9.25	275	2.0	910

TABLE VII - Critical Properties of BeO and Graphite Reflectors at Core Radius=15 cm.

Reflector thickness	BeO Critical U conc.	M^{25}	K	S	C Conc.	M^{25}	K	S
10 cm	39.6	560	1.57	9.9	76.3	1080	1.79	5.9
20	31.6	447	1.48	12.5	52.3	740	1.68	7.8
30	29.6	419	1.45	13.4	-	-	-	-
50	-	-	-	-	40.8	577	1.59	9.6
∞	28.4	401	1.43	14.0	38.0	537	1.56	10.3

Here, M^{25} is the critical mass, K the reproduction constant of the core, and S the reflector savings in cm.

From the preceding tables, we deduce the following information:

1) The optimum core radius is around 12 cm for minimum critical mass in C and the mass in any case is not too sensitive to this parameter.

2) The first 10 cm of BeO have a strikingly larger reflector effect than the

same amount of graphite; the increment on adding more reflector is about the same for BeO and C.

We therefore computed the critical mass of a three region system with a 12 cm radius core, a 10 cm thick BeO shell, and an infinite graphite outer reflector. This system turned out to have a phenomenally small critical mass: 332 g U^{235}, at a concentration of 46 g^{25}/liter.

Table VIII and Figure 5 give estimates of the flux and power characteristics of the system with 12 cm radius core, 10 cm of BeO, and ∞C.

Figure 5 gives the fast $\int_{E_{Thermal}}^{\infty} \varphi(E)dE$ and thermal fluxes and their ratio. The two-group theory used here overestimates epithermal flux at large distances, and hence the flux ratio increases more rapidly than indicated.

Table VIII lists the flux available at r = 100 from various core fluxes and powers.

TABLE VIII

$\bar{\varphi}$ core	Power (Watts)	φ(100 cm)
10^5	1.6×10^{-3}	5×10^3
10^6	1.6×10^{-2}	5×10^4
10^7	.16	5×10^5
10^8	1.6	5×10^6
10^9	16	5×10^7
10^{10}	160	5×10^8

It is seen that a 50-watt limitation would give a rather high thermal flux at reasonable Cd ratio for routine experimentation. Even a 1 watt limit would provide a reasonable flux as an exponential assembly or meter testing source.

Figure 6 is similar to Figure 5, except that the core is 12.7 cm in radius and the reflector contains no BeO. This system is the minimum critical mass configuration for an ∞ graphite reflector.

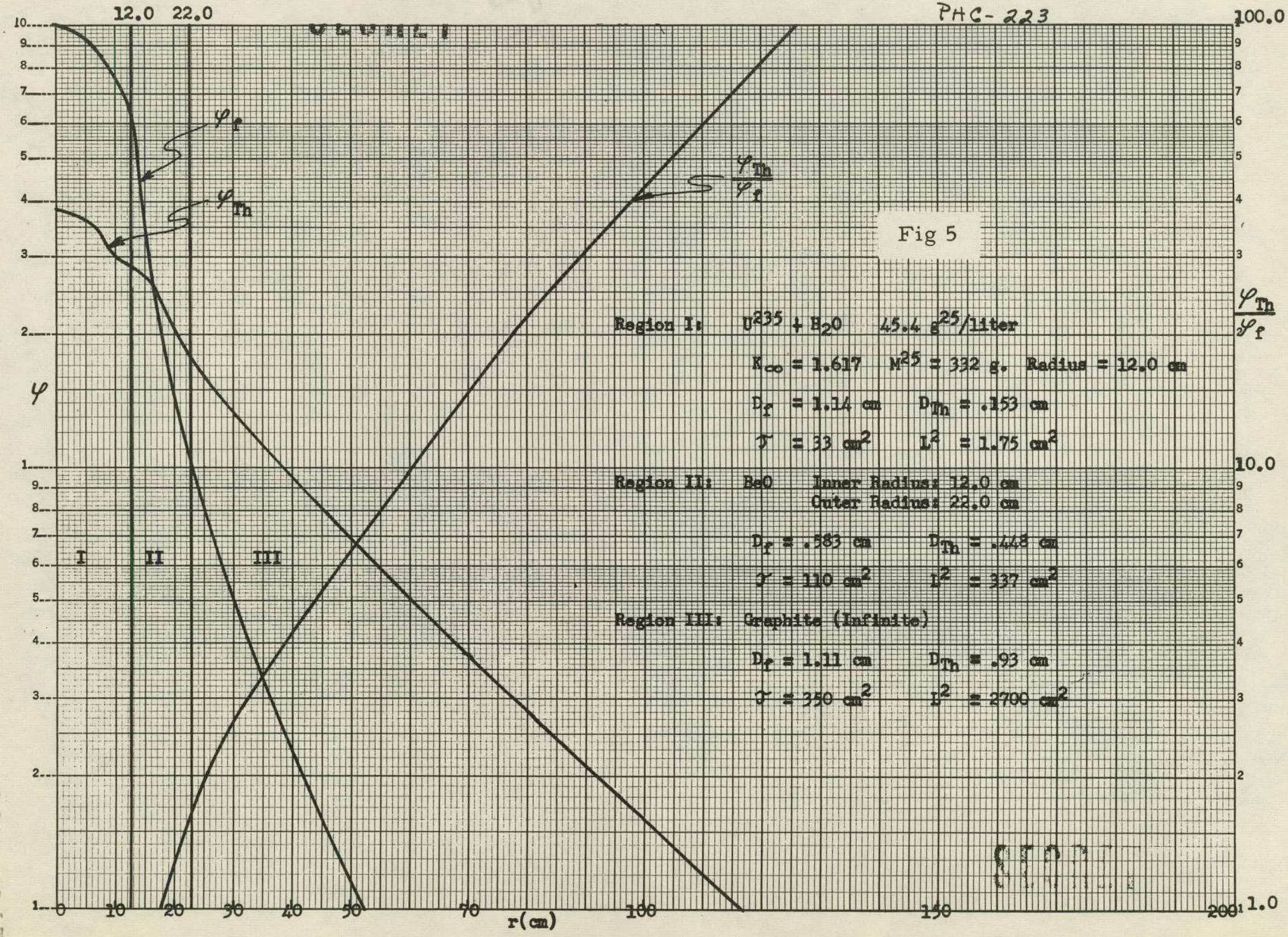

Fig 5

Region I: $U^{235} + H_2O$ 45.4 g^{25}/liter

$K_{\infty} = 1.617$ $M^{25} = 332$ g. Radius = 12.0 cm

$D_f = 1.14$ cm $D_{Th} = .153$ cm

$\tau = 33$ cm^2 $L^2 = 1.75$ cm^2

Region II: BeO Inner Radius: 12.0 cm
Outer Radius: 22.0 cm

$D_f = .583$ cm $D_{Th} = .448$ cm

$\tau = 110$ cm^2 $L^2 = 337$ cm^2

Region III: Graphite (Infinite)

$D_f = 1.11$ cm $D_{Th} = .93$ cm

$\tau = 350$ cm^2 $L^2 = 2700$ cm^2

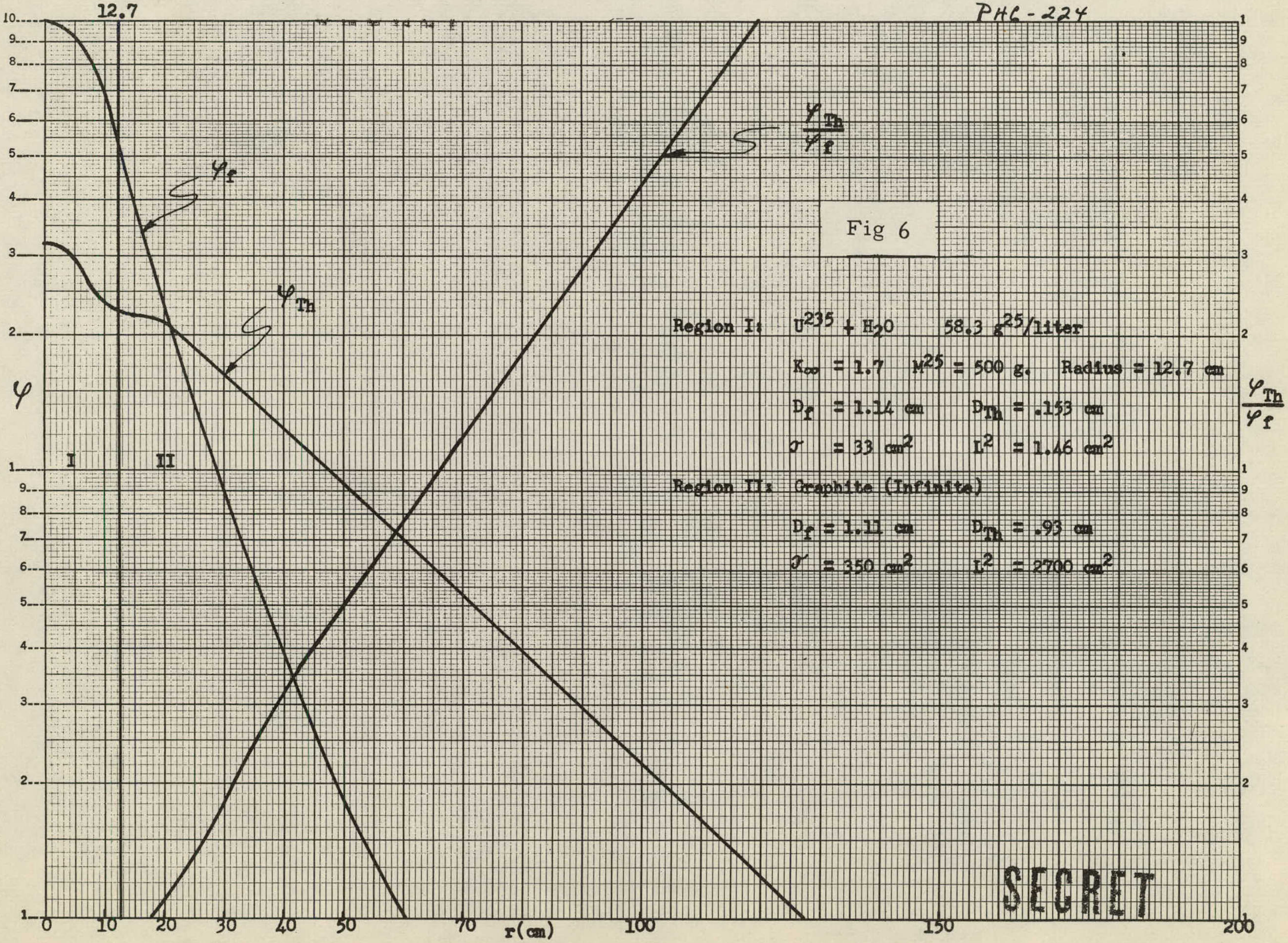

Fig 6

Argument

There are many experiments with neutrons for which high fluxes are of dubious advantage. Such are:

1) Sources for exponential experiments.

2) Sources for biological experiments.

3) Danger-coefficient cross section testing.

4) Foil calibrations and meter testing.

5) Activation of high cross section materials.

For most of these purposes, flux levels of 10^5 - 10^9 are adequate. These flux levels are attainable in critical systems without generation of appreciable power. Higher flux levels involve the generation and removal of power, with attendant construction difficulties and increased cost, as well as greater shielding.

The usual low power test reactors, such as CP-2 and W-305 are adequate systems for these purposes. However, due to the use of natural U fuel, their critical masses are large, and the consequence is that even at 10^5 thermal column flux the reactor power, while small, is enough to require a cooling system. Furthermore, each of these reactors consists of a single critical system; hence, if more than one experiment is to be performed at a time, the experimenters must compromise on use of facilities and on operating flux. Certain experiments (danger coefficient testing, for example) preclude simultaneous operation.

In place of single large natural uranium units, a number of smaller enriched units might be constructed. It is desirable that such units should be flux or power limited, constructed without any cooling system, safe, and of small cost. For economy of enriched fissionable material, safety, and ease of construction, the water-boiler types offer a promising point of departure.

From previous work at Los Alamos and other places, we have considerable information as to their properties, and the above calculations show that significant reduction in quantity of fuel over that in the Y boiler may be achieved. The small critical mass is a safety factor, in that any change in geometry tends to lower the reactivity; moreover, because of the small total absorption of the system, miniature control systems should be workable.

It is proposed that critical assemblies be tested to check whether these low masses of fuel can be made critical; and if so, that at least three uncomplicated experimental units be designed and constructed.

XI. Cross-Sections for Inelastic Scattering of Neutrons by Middle-Weight Nuclei with Excitation of Single Levels. J. E. Monahan

For energies such that only one level of the residual nucleus can be excited, the neutron inelastic cross section is given by Feld et al.[1], as:

$$\sigma_{in}(iE|\bar{i}\bar{E}) = \frac{\pi\lambda^2}{2(2i+1)} \sum_{\ell} T_{\ell}(E) \sum_{J} \frac{\epsilon^{J}_{j\ell}\,(2J+1)}{1 + \dfrac{\sum_{j'} \epsilon^{J}_{j'\ell'} T_{\ell'}(E)}{\sum_{j} \epsilon^{J}_{j\ell} T_{\ell}(E)}} \qquad (1)$$

where (E,ℓ) and $(\bar{E},\bar{\ell})$ are the initial and final energies and orbital angular momenta of the neutron, J is the spin of the compound nucleus, and

$$j_{1,2} = i \pm \tfrac{1}{2} \quad ; \quad \bar{j}_{1,2} = \bar{i} \pm \tfrac{1}{2}$$

are the so-called channel spins; i and $\bar{i}$ denote the initial and final spins of the scattering nucleus. The quantities $\epsilon^{J}_{j\ell}$ equal 1 or 2 depending on whether one or both values of the channel spin satisfy the inequality $|J-\ell| \leq j_i \leq J+\ell$. The penetrabilities T_ℓ are defined by the expression

$$T_{\ell} = \frac{4kK\,|u_{\ell}(R)|^{-2}}{K^2 + 2kK\,|u_{\ell}(R)|^{-2} + \dfrac{du_{\ell}(R)/dR}{u_{\ell}(R)}},$$

where

$$k = \lambda^{-1} = \frac{(2mE)^{1/2}}{\hbar}$$

and

$$K^2 = K_c^2 + k^2$$

$$u_{\ell}(R) = i\left(\frac{\pi kR}{2}\right)^{1/2} H^{(1)}_{\ell+\frac{1}{2}}(kR).$$

The internal wave-number K_c is defined as the wave-number of a neutron which enters the nucleus with zero kinetic energy; a theoretical estimate[2] yields the value $K_c = 10^{13}\ cm^{-1}$. The nuclear radius R, which is a function of E, can be obtained by total cross-section measurements. For a given l, the sums are over all J, ℓ', and $\bar{\ell}$ which conserve momentum and parity.

C85 C49

If the energy of the incident neutron is sufficient to excite more than

1. B. Feld, H. Feshbach, M. Goldberger, H. Goldstein, and V. Weisskopf; "Final Report of Fast Neutron Data Project" USAEC Report NYO-636.
2. H. Feshbach, D. Peaslee, and V. Weisskopf, Phys. Rev. 76, 1550, (1949).

one level of the residual nucleus, the cross-section for excitation of the level ($E - \bar{E}, \bar{i}$) is given by equation (1) after the summation over ℓ' is replaced by

$$\sum_{j_i, E_i, \ell_i'} \epsilon^{J}_{j_i \ell_i'} T_{\ell_i'}(E_i) \qquad (2)$$

This sum is to include all competing levels except the one to which the decay proceeds.

Basic in the derivation of these formulae are the assumptions that only neutron emission is possible and that the spacing of energy levels in the compound nucleus is small compared with their widths at excitation energies corresponding to the energy of the incident neutron. Further, the formula resulting from equation (2) is of practical value only for reactions involving two or three excitation levels. These conditions are very nearly satisfied for neutron energies just above the first excited levels of most middle-weight and heavy "magic" nuclei.

Some calculations based on equation (1) have been published;[1] these, however, were limited to an extremely unfavorable transition at comparatively low energies. Compared with the corresponding total cross-sections, the resulting inelastic cross-sections are negligibly small. It seems worthwhile, therefore, to extend these computations to higher energies and to include more favorable reactions.

The following curves represent the results of an attempt to determine the order of magnitude of the inelastic cross-section in the range of applicability of equation (1). While the combination of parameters R, E, $\bar{E}$, i, and $\bar{i}$ chosen do not represent any particular scattering process, an attempt was made to assign values which are representative of middle-weight nuclei. Curves 7 through 12 represent the cross-section for excitation of the level

1. B. Feld, H. Feshbach, M. Goldberger, H. Goldstein, and V. Weisskopf; "Final Report of Fast Neutron Data Project" USAEC Report NYO-636.

($E - \bar{E}$ as a function of E provided no other level can be excited in this energy interval. The spin and relative parity of the excited state associated with each curve is listed. The two remaining curves, Figs. 13 and 14 correspond to processes in which two levels can be excited; $\sigma_{II}(E_i)$ denotes the cross-section for excitation of the single level; E_i when a second level also can be excited. The curves labeled $\sigma_I(E_i)$ give the corresponding single-level cross-sections reproduced from the first set of curves in order to facilitate comparison.

A few calculations for higher ground state spins are given in the table.

$R = 5 \times 10^{-13}$ cm; $E - \bar{E} = 0.8$ Mev; $i = 2$

E (Mev)	$\bar{i}$	(barns)	E (Mev)	$\bar{i}$	(barns)
0.85	0+	0.015	2.20	2+	0.506
0.85	0-	0.021	2.20	2-	0.488
2.20	0+	0.125	0.85	3+	0.129
2.20	0-	0.120	0.85	3-	0.160
0.85	1+	0.065	2.20	3+	0.520
0.85	1-	0.072	2.20	3-	0.584
2.20	1+	0.316	0.85	4+	0.094
2.20	1-	0.316	0.85	4-	0.086
0.85	2+	0.127	2.20	4+	0.414
0.85	2-	0.128	2.20	4-	0.395

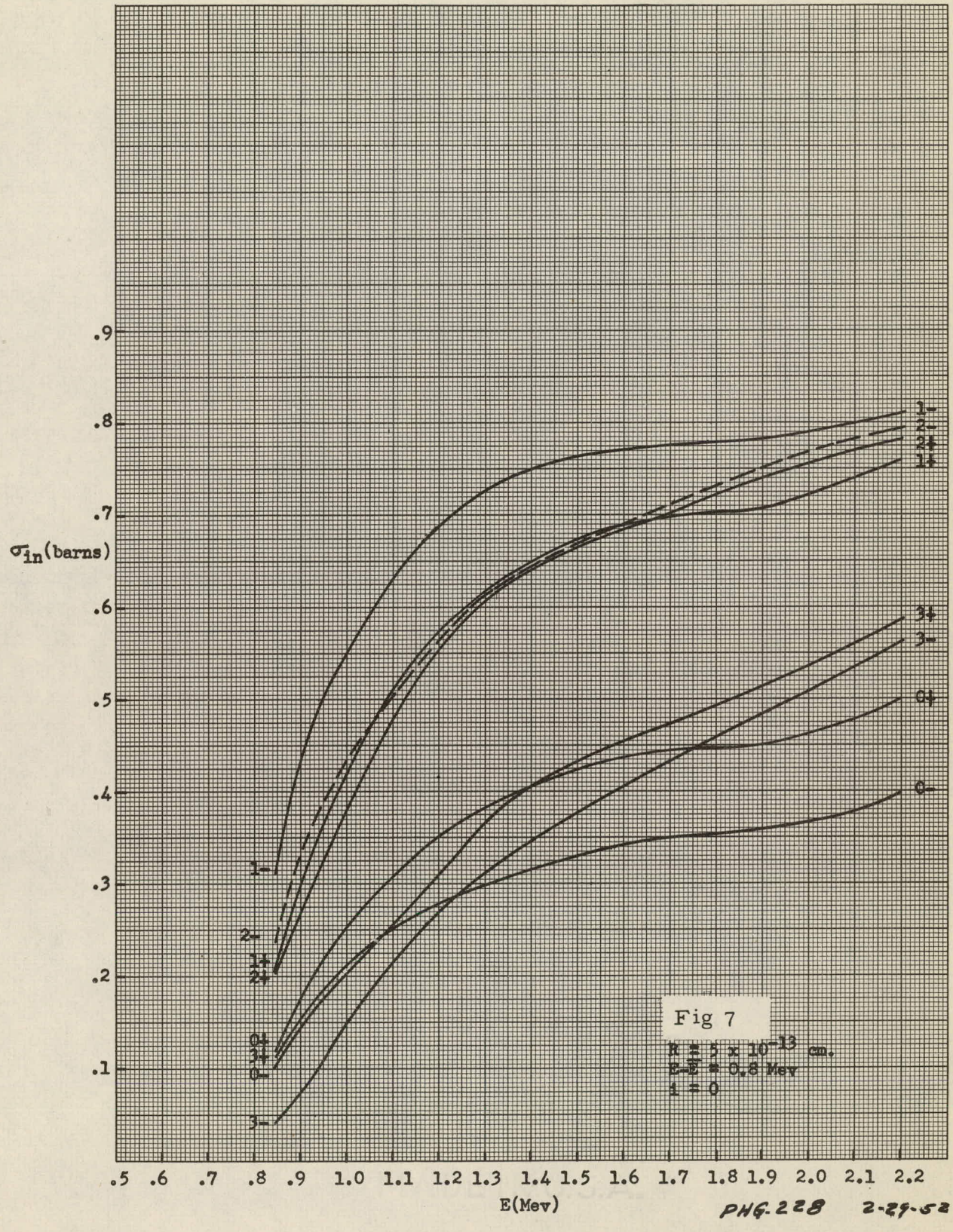

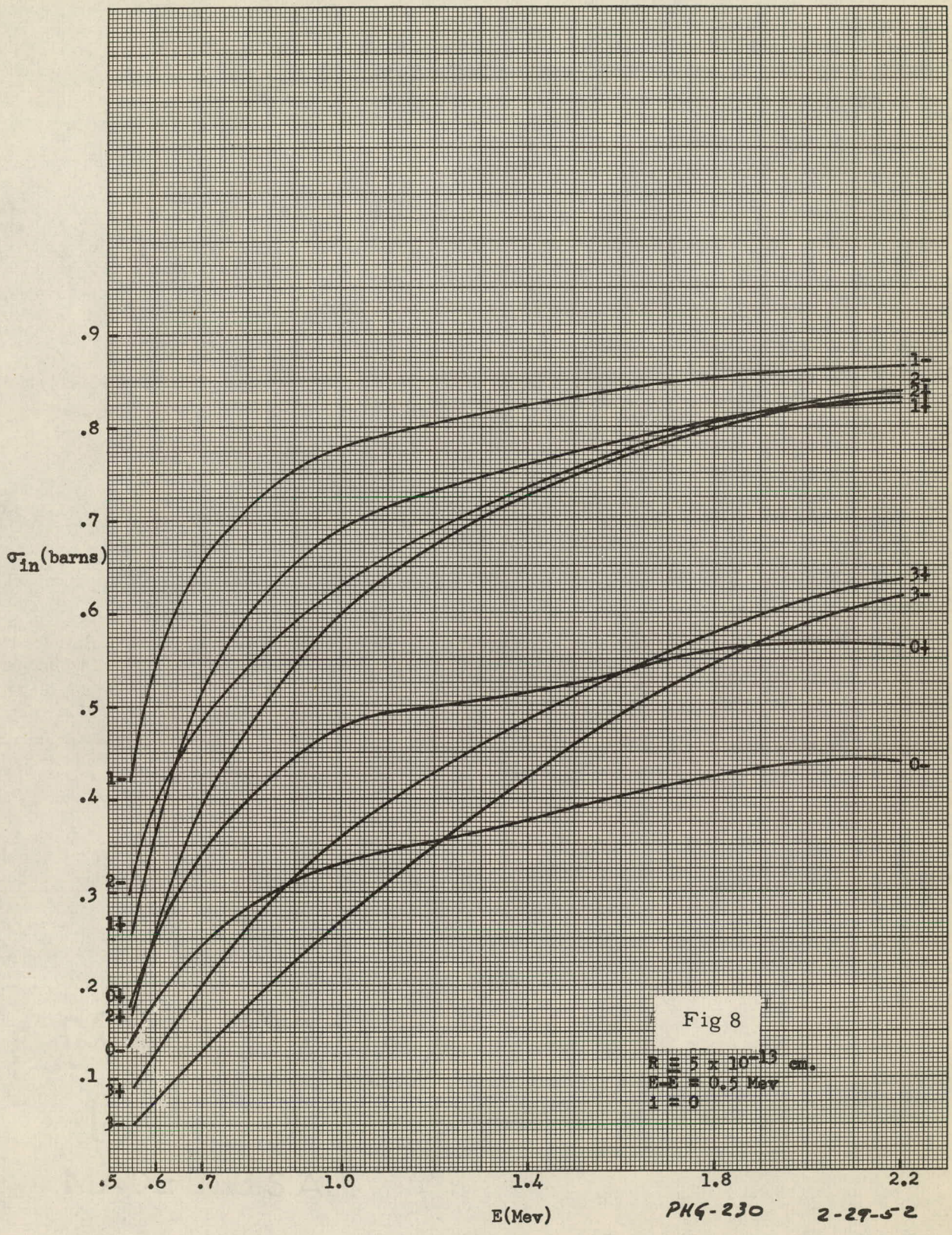

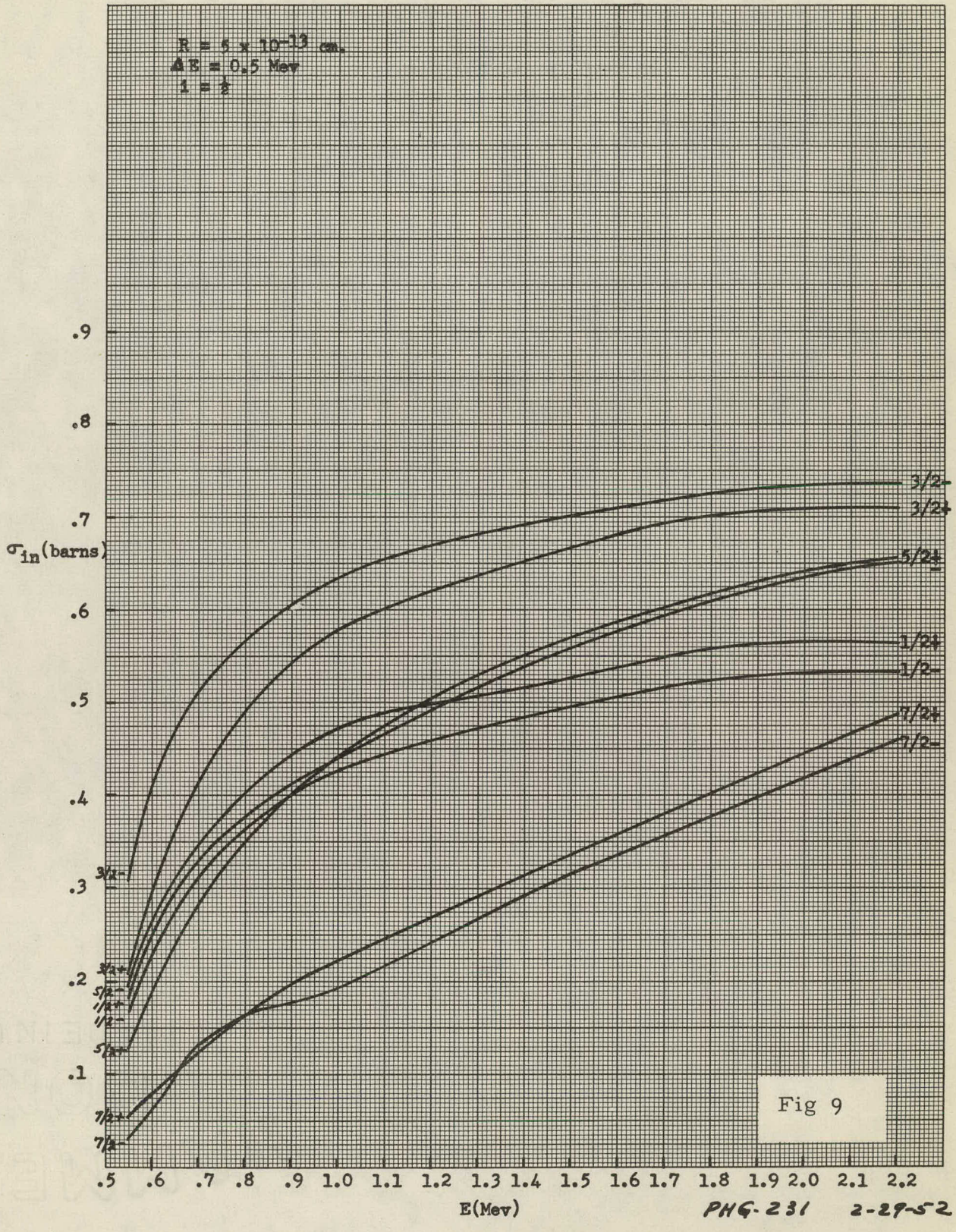

Fig 9

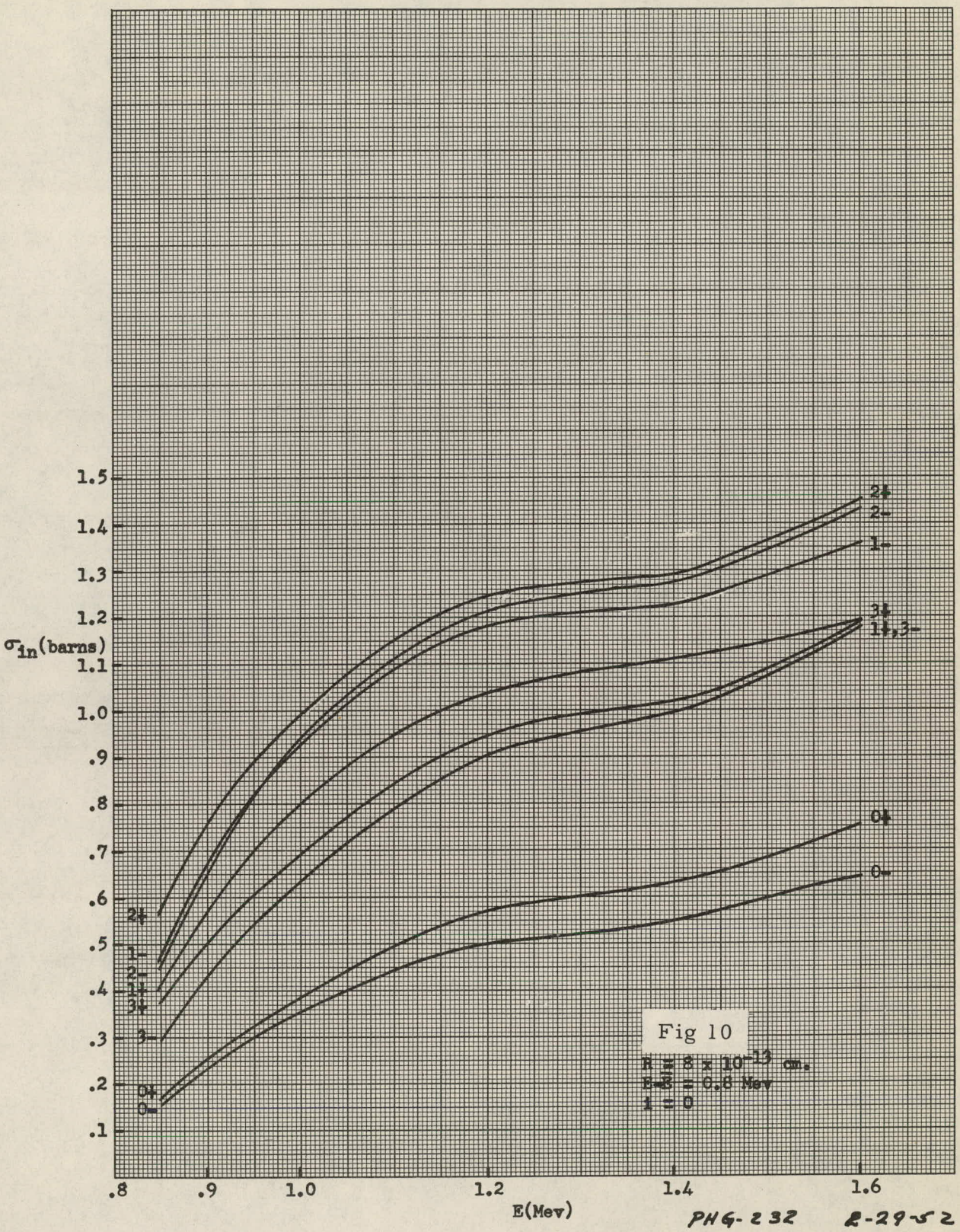

Fig 10

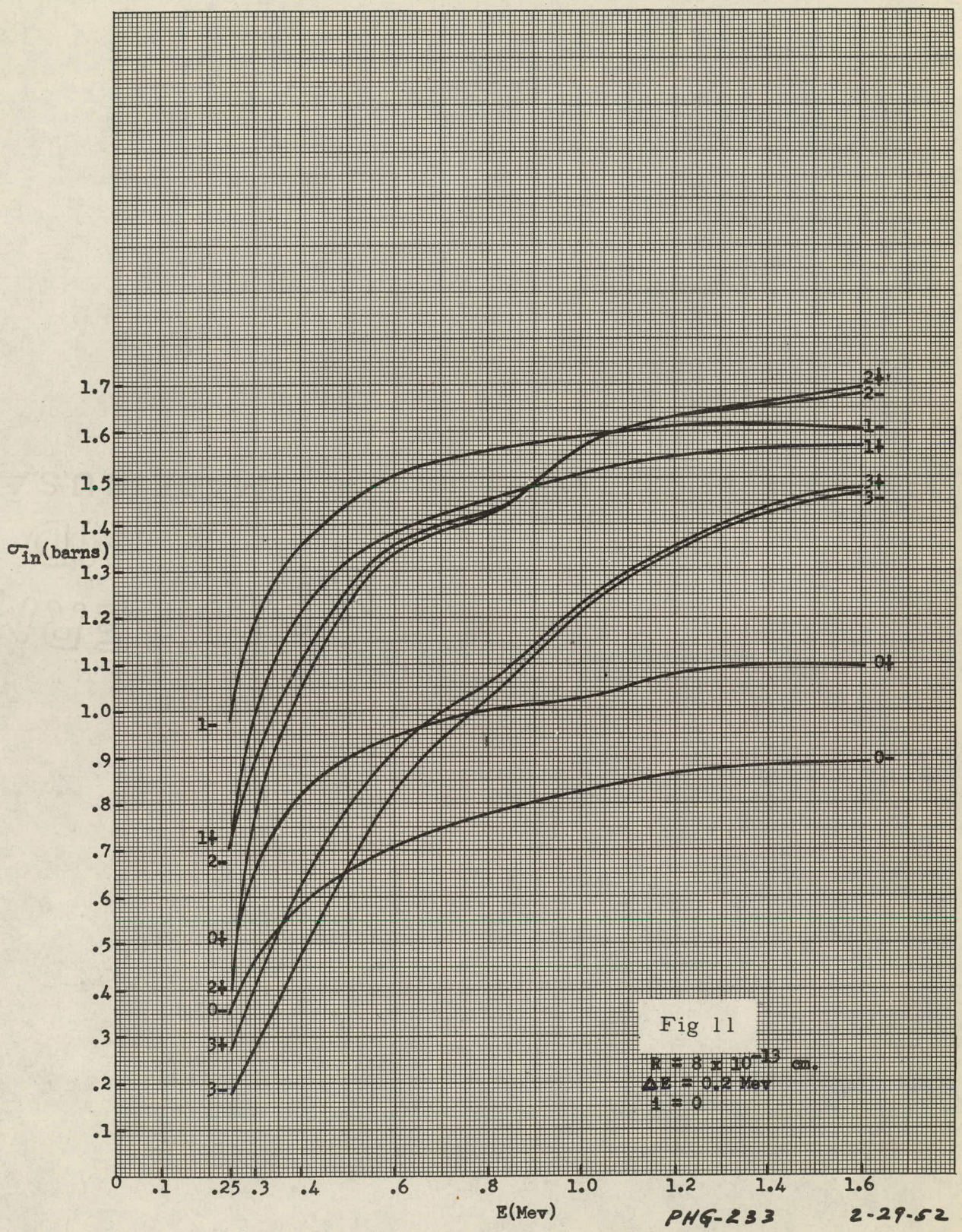

Fig 11

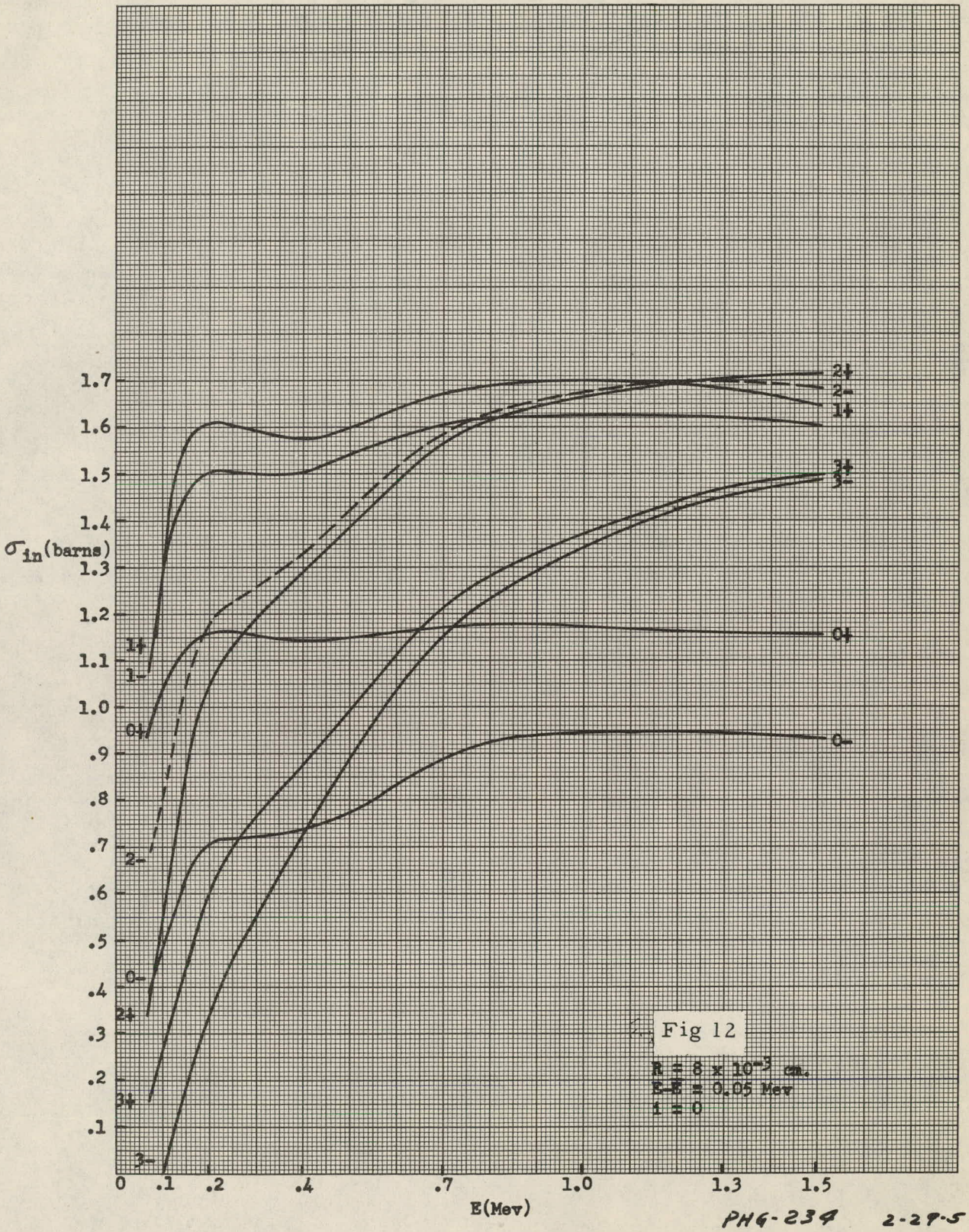

Fig 12

PHG-234 2-29-52

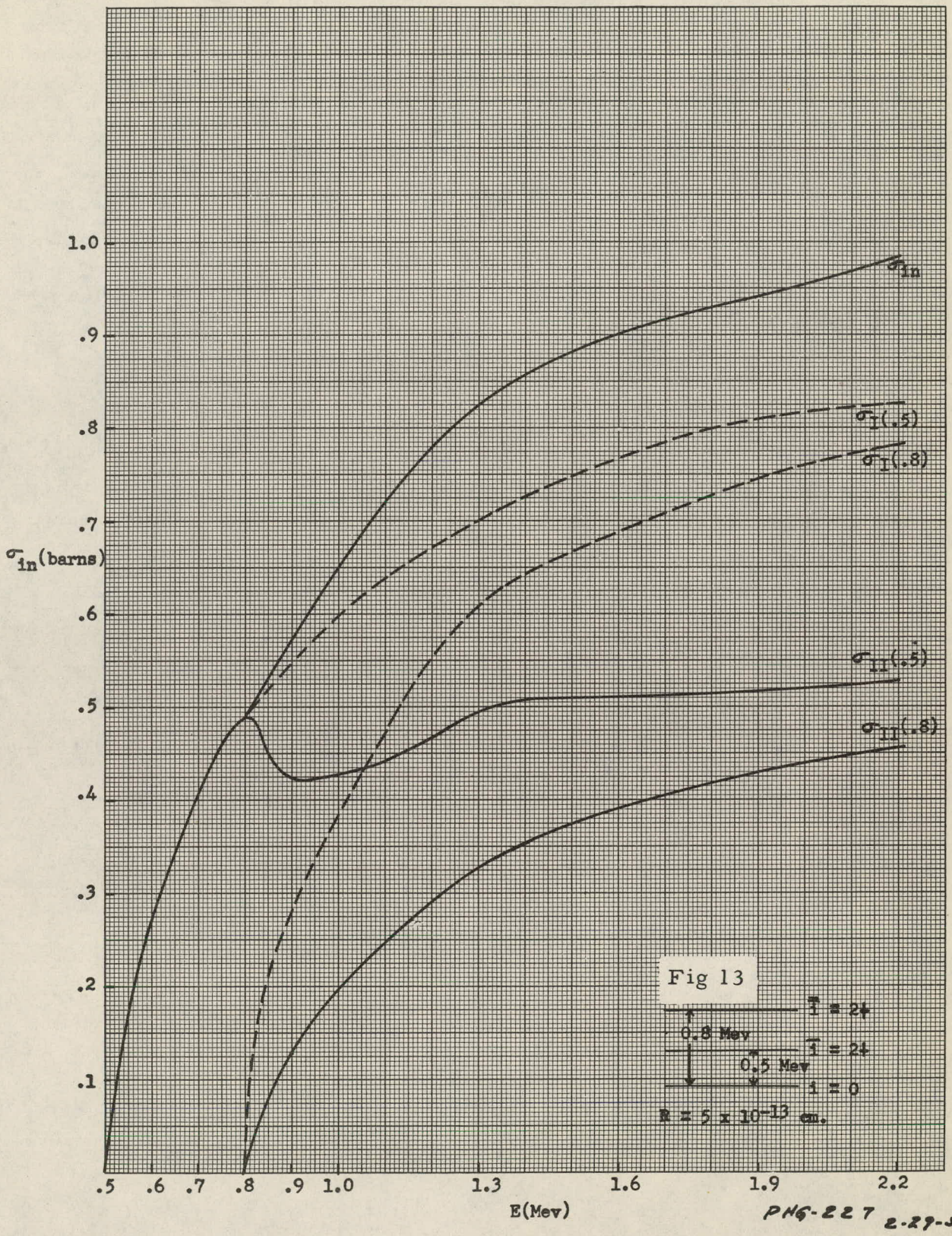

Fig 13

PNG-227 2-27-52

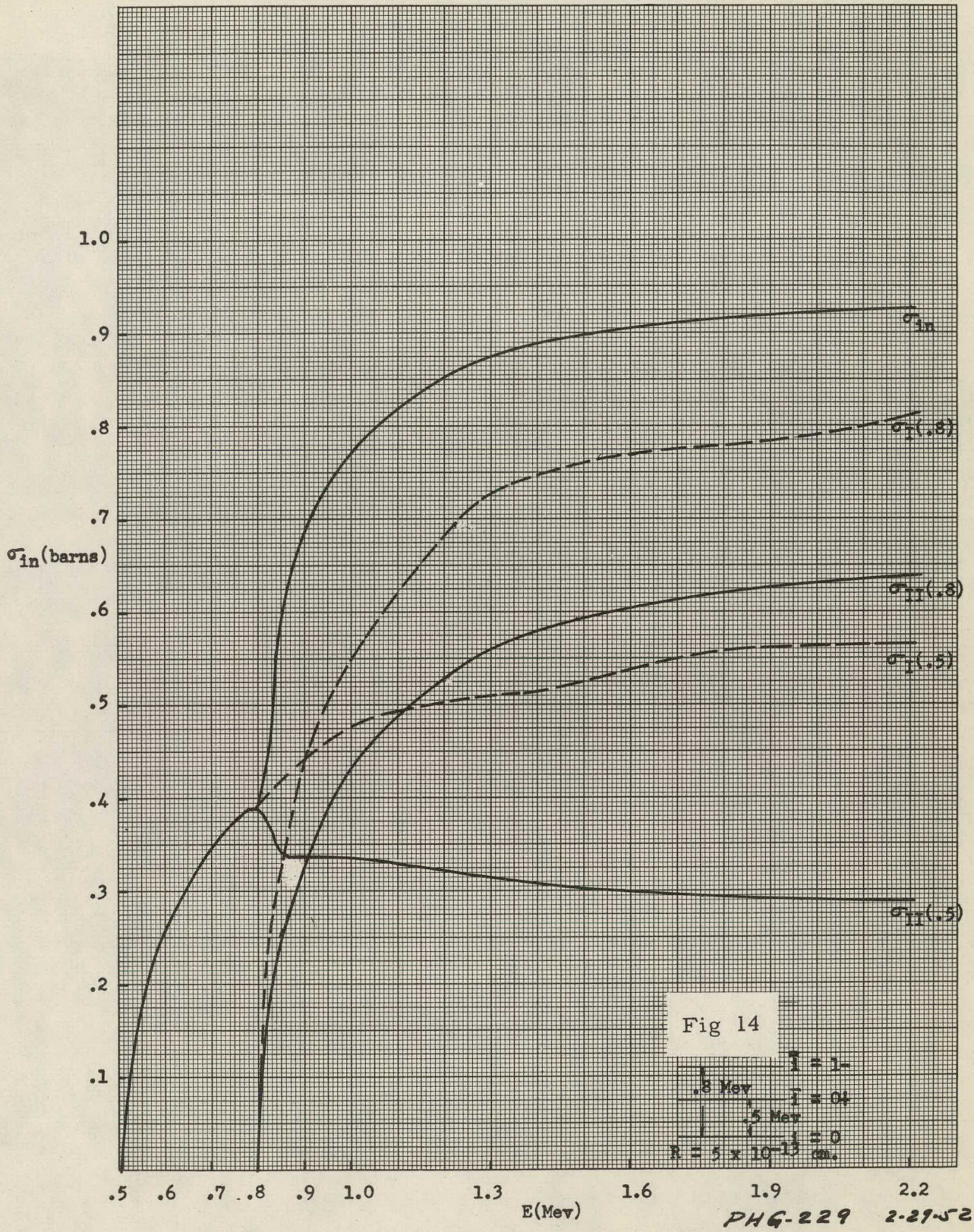

XII. Spin of K^{40} and Cl^{36} Nuclei from the jj-coupling Model - D. Kurath

The order of energy levels for K^{40} $\left[(1f_{7/2})^1 \ (1d_{3/2})^{-1}\right]$ and Cl^{36} $\left[(1d_{3/2})^1 \ (1d_{3/2})^{-1}\right]$ has been investigated using jj-coupled wave functions. The individual particles are represented as moving in a central oscillator potential. The splitting of the possible angular momentum states under the perturbation of a nucleon interaction consisting of a Gaussian potential

$$V(r_{12}) = A\, e^{-(r_{12}/r_0)^2}$$

multiplied by various exchange operators was treated. The general central interaction potential is a linear combination:

$$J_{12} = \left[W(1) + M(P_{12}) + B(Q_{12}) + H(P_{12}Q_{12})\right] V(r_{12})$$

where the operators P_{12} and Q_{12} are space and ordinary-spin exchange operators respectively. The coefficients stand for the names associated with each type, Wigner, Majorana, Bartlett and Heisenberg in order.

The necessary integrals were obtained by expanding the Gaussian potential in terms of the Legendre polynomials:

$$V(r_{12}) = \sum_{k=0}^{l+l'} (2k+1)\, V_k(r_1, r_2)\, P_k(\cos\theta_{12})$$

and then calculating the Slater integrals:

$$F_k = \int_0^\infty \int_0^\infty R_l(r_1)\, R_{l'}(r_2)\, J_{12}\, R_l(r_1)\, R_{l'}(r_2)\, r_1^2\, r_2^2\, dr_1\, dr_2 \ .$$

Here l and l' are the orbital angular momenta of the particles, J_{12} is the interaction potential, and R_l and $R_{l'}$ are the radial parts of the individual particle wave functions, normalized:

$$\int_0^\infty R_l^2(r)\, r^2\, dr = 1$$

For the nuclei treated we have two functions:

$$R_d = \text{const.}\, r^2\, e^{-(r/r_d)^2}$$

$$R_f = \text{const.}\, r^3\, e^{-(r/r_f)^2}$$

where r_d and r_f are parameters connected with the nuclear radius. The angular part of the integrations can be taken from Table 1[b] of Condon and Shortley, "Theory of Atomic Spectra" where the same procedure is used for Coulomb forces.

The ground state is given in the tables below as a function of the ratio of parameters, (r_d/r_0), for each exchange type. In K^{40} the assumption $r_f \approx r_d$ has been made.

K^{40}

J →	2	3	4	5	Degeneracies
W	—	—	$r_d/r_0 > 0$	—	all deg. at 0
M	—	—	$r_d/r_0 > 1.31$	$r_d/r_0 < 1.31$	—
H	$r_d/r_0 > 0$	—	$r_d/r_0 > 0$	—	2,4 deg.; all deg. at 0
B	$r_d/r_0 < \infty$	—	—	—	2,4 deg. at ∞

Cl^{36}

J →	0	1	2	3	Degeneracies
W	—	—	$r_d/r_0 > 0$	—	all deg. at 0
M	—	—	$r_d/r_0 > 1.46$	$r_d/r_0 < 1.46$	2,3 deg. at 0
H	—	$r_d/r_0 > 0$	—	$r_d/r_0 > 0$	1,3 deg.; 1,2,3 deg. at 0
B	—	—	—	$r_d/r_0 < \infty$	1,3 deg. at ∞

Space dependent forces (W and M) are expected to be present to about four times the extent of spin dependent forces (B and H), so their result should carry greater weight. However, while they behave essentially the same way for both nuclei in that they would give $J = j + j'$ or $J = j + j' - 1$, the spin dependent forces differ for the two cases. They tend to strengthen the result $J = j + j' - 1 = 4$ for K^{40}, and $J = j + j' = 3$ for Cl^{36}. Thus, the value of (r_d/r_0) for which $J = j + j'$ and $J = j + j' - 1$ cross would be considerably larger for Cl^{36}.

Since one expects r_d/r_0 to be about 1.0 to 1.5, one would expect $J = 4$ for K^{40} and $J = 2$ or 3 for Cl^{36}. The experimental results are $J = 4$ for K^{40} and $J = 2$ for Cl^{36}.

The result for delta-function range dependence seems to be part of a general rule that for one particle and one hole the resultant spin is:

$$J = j + j' - 1$$

which should be more likely to hold as larger nuclei are considered where the delta function approximation should be better.

XIII. Quadrupole Moments and Nuclear Deformability M. G. Mayer

The magnitude of the nuclear quadrupole moments has been explained by Rainwater as being due to the deformation of the nucleus by the centrifugal force of the odd nucleon. By using a straightforward perturbation method it is possible to determine nuclear deformabilities from the empirical quadrupole moments. These deformabilities, plotted against neutron number, lie reasonably well on one curve. On the average, the deformability is much higher than that obtained from the empirical Bohr-Wheeler formula. At closed shells of neutrons, the deformability seems to drop to zero. Closed shells of protons have no influence.

XIV. Magnetic Moments of Nuclei M. G. Mayer

It was noticed that the assumption of spin-orbit coupling in nuclei gives rise to additional electromagnetic interactions. Due to this effect the magnetic moments of odd proton nuclei should not lie on the theoretical "Schmidt lines", but in between them. The effect is, however, much too small to explain the observed deviations.

XV. Interaction Between the Configurations $d^{n-2}sp$ and $d^{n-1}p$ (iron group)
N. Rosenzweig

1. Introduction The customary approach to a theoretical understanding of the spectrum of an element in the iron group consists of constructing the matrix of the electrostatic interaction in the Russell-Saunders (SL) scheme. The matrix components are expressed in terms of Slater integrals (the various types of integrals being small in number compared to the number of eigen-values of the matrix).

In order to account fully for the observed terms, the Russell-Saunders scheme must include not only the configuration label and SL values but also other quantum numbers. For example, the low-lying odd terms of a typical iron group spectrum are obtained in the space of the two configurations $d^{n-2}sp$ and d^{n-1} (Fig. 15) and the following additional quantum numbers: α_1, S_1 L_1 representing respectively seniority number,[1] and orbital angular momentum of d^{n-2} group; S_2 spin of d^{n-2} group; SL of $d^{n-2}sp$ group; $\alpha_3 S_3 L_3$ of d^{n-1} group and SL of $d^{n-1}p$ group.

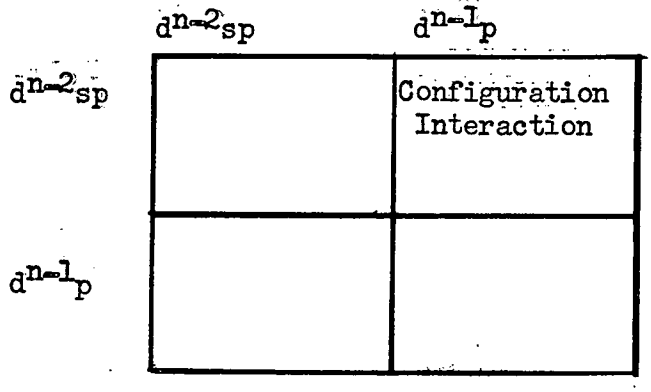

Fig. 15 Schematic Diagram of Energy Matrix

The presumption that the matrix elements in the off-diagonal blocks of the matrix (see Fig. 15) are negligibly small is often not justified, and these elements must in fact be considered in the calculation. This means that the

1. G. Racah, Phys. Rev. 63, 367 (1943) denoted by RIII.

general off-diagonal matrix component C,

$$C = \left[d^{n-2} \alpha_1 S_1 L_1 \; s \; S_2 L_2 \; p \; SL \middle| \sum_{i<j} \frac{e^2}{r_{ij}} \middle| d^{n-1} \alpha_3 S_3 L_3 \; p \; SL \right] \quad \ldots (1)$$

must be expressed in terms of Slater integrals. This has been done, the remaining parts of this report being an outline of this reduction. The results in a form suitable for ready application to the spectrum of every element in the iron group will be submitted to the Physical Review for publication.

2. Expanded forms of wave functions. The wave functions

$$\Psi[\ell^{n-2} \alpha_1 S_1 L_1 \; \ell' S_2 L_2 \; \ell'' SL] \text{ and } \Psi[\ell^{n-1} \alpha_3 S_3 L_3 \; \ell'' SL]$$

are antisymmetric in all n electrons and are built up from one-electron functions in the usual fashion: The groups of equivalent electrons are formed by means of the coefficients of fractional parentage[1] and the usual vector coupling formulas. The inequivalent electrons are added by the usual vector coupling formulas.

We shall succeed in reducing (1) to the desired form by showing explicitly the construction of the wave functions. Free use will be made of the following expanded forms.

(a) Antisymmetrizing with respect to the last electron.

$$\Psi[\ell^{n-1} \alpha_3 S_3 L_3 \cdot \ell'' SL] = \frac{1}{\sqrt{n}} \sum_{q=1}^{n} (-1)^Q \Psi[\ell^{n-1} \alpha_3 S_3 L_3 \cdot \ell_q'' SL]$$

Q is the parity of the permutation which exchanges q with n.

(b) Addition of two angular momenta.

$$\Psi[\ell^{n-1} \alpha_3 S_3 L_3 \cdot \ell_q'' SL] = \sum_{\substack{M_{S_3} M_{L_3} \\ m_{\ell''} m_{s''}}} \Psi[\ell^{n-1} \alpha_3 S_3 L_3 M_{S_3} M_{L_3}] \, \phi[n'' \ell'' m_{\ell''} m_{s''}] \times [M_{S_3} M_{L_3} m_{s''} m_{\ell''} / M_S M_L SL]$$

The coefficients of the transformation are known, but we shall need only the general properties of the unitary transformation.

1. G. Racah, Phys. Rev. 63, 367 (1943) denoted by R III.

(c) Expansion in terms of fractional parents[1].

$$\psi[l^{n-1}\alpha_3 S_3 L_3] = \sum_{\alpha_3' S_3' L_3'} \psi[l^{n-2}\alpha_3' S_3' L_3' l_{n-1} S_3 L_3][l^{n-2}\alpha_3' S_3' L_3' l S_3 L_3 \} l^{n-1}\alpha_3 S_3 L_3]$$

The coefficients for d^n are given in R III for n = 1 to 5 (left side of periodic table). These results can readily be extended to the right side n = 6 to 10.

(d) Coupling of three angular momenta.

$$\psi[l^{n-1}\alpha_3' S_3' L_3' l_{n-1} S_3 L_3 l_q'' SL] = \sum_{S_4 L_4} \psi[l^{n-1}\alpha_3' S_3' L_3' \cdot l_{n-1} l_q''(S_4 L_4) SL] \times [S_3' L_3' l l''(S_4 L_4) SL | S_3' L_3' l(S_3 L_3) l'' S L]$$

The coefficients are expressible in terms of the W function[2] (R II) and are, therefore, readily calculated.

$$\psi[l^{n-2}\alpha_1 S_1 L_1 l' S_2 L_2 l'' S L]$$

is constructed in a similar fashion.

3. Reduction of C. In view of the symmetry of the operator $\sum_{i,j} \frac{e^2}{r_{ij}}$ and the antisymmetry of the states

$$C = \frac{n(n-1)}{2}[l^{n-2}\alpha_1 S_1 L_1 l' S_2 L_2 l'' S L | \frac{e^2}{r_{n,n-1}} | l^{n-1}\alpha_3 S_3 L_3 l'' S L]. \quad (2)$$

Exhibiting the antisymmetrization with respect to the last electron on both left and right in the manner (a) we have

$$C = \frac{(n-1)}{2} \sum_{p,q=1}^{n} (-1)^{p+q} [l^{n-2}\alpha_1 S_1 L_1 l' S_2 L_2 l_p'' S L | \frac{e^2}{r_{n,n-1}} | l^{n-1}\alpha_3 S_3 L_3 l_q'' S L] \quad (3).$$

---

1. G. Racah, Phys. Rev. 63, 367 (1943) denoted by RIII.
2. G. Racah, Phys. Rev. 62, 438 (1942) denoted by RII.

Expression (3) is a sum of n^2 terms. A suitable grouping is the following:

(i) C' $p = n, n-1$ with $q = 1, 2, \ldots n-2$
$p = 1, 2 \ldots n-2$ with $q = n, n-1$

(ii) C'' $p = 1, 2, \ldots n-2$; $q = 1, 2 \ldots n-2$.

(iii) C''' $p = n, n-1$; $q = n, n-1$

The above is a complete enumeration and therefore

$$C = C^{I} + C^{II} + C^{III} \qquad (4).$$

We shall consider one at a time.

(i) In each term of C' one and only one of either ℓ_p'' of ℓ_q'' is involved in the integration with the operator. The other one is orthogonal to the part of the wave-function, the coordinates of which are different from those of the operator. Therefore, each term of C' vanishes.

(ii) Neither ℓ_p'' nor ℓ_q'' has the same coordinates as the operator. Therefore, the terms of C'' vanish unless $p = q$. Note also that $(-1)^{P+Q} = 1$ for all non-vanishing terms. There are thus n-2 terms which are all equal. Thus

$$C'' = \frac{(n-1)(n-2)}{2}\left[\ell^{n-2}\alpha_1 S_1 L_1 \ell' S_2 L_2 \ell_1'' SL \middle| \frac{e^2}{r_{n,n-1}} \middle| \ell^{n-1}\alpha_3 S_3 L_3 \ell_1'' SL\right] \qquad (5).$$

The expression (5) is simplified by considering the coupling of the ℓ'' electron to the parent angular momenta in the manner (b). Keeping in mind 1) that the electrostatic interaction is diagonal with respect to total spin and orbital angular momentum and 2) and the unitary character of the coupling leads to

$$C'' = \left[l^{n-2} \alpha_1 S_1 L_1 \, l' S_2 L_2 \middle| \sum_{i<j}^{n} \frac{e^2}{r_{ij}} \middle| l^{n-1} \alpha_3 S_3 L_3 \right] \delta(S_2 S_3) \delta(L_2 L_3) \quad (6).$$

Thus C'' is precisely the matrix component of the electrostatic interaction between the parent configurations. Since these elements have been discussed fully in R III, we turn our attention to C'''.

(iii) It is convenient to subdivide C''' as follows:

C_1''' $\quad p = n \quad q = n$

C_2''' $\quad p = n-1 \quad q = n-1$

C_3''' $\quad p = n-1 \quad q = n$

C_4''' $\quad p = n \quad q = n-1$

$$C''' = C_1''' + C_2''' + C_3''' + C_4'''$$

Inspecting (2) it is clear that $C_1''' = C_2'''$ and $C_3''' = C_4'''$. However, we shall see that C_1''' and C_3''' differ significantly.

Let us study C_1''' first. $(-1)^{P+Q} = 1$. Thus

$$\frac{2}{(n-1)} C_1''' = \left[l^{n-2} \alpha_1 S_1 L_1 \, l' S_2 L_2 \, l_n'' SL \middle| \frac{e^2}{r_{n,n-1}} \middle| l^{n-1} \alpha_3 S_3 L_3 \, l_n'' SL \right] \quad (7).$$

Considering the antisymmetrization of the l' electron and its orthogonality to the wave function on the right leads to

$$\frac{2}{\sqrt{n-1}} C_1''' = \left[l^{n-2} \alpha_1 S_1 L_1 \, l_{n-1}' S_2 L_2 \, l_n'' SL \middle| \frac{e^2}{r_{n,n-1}} \middle| l^{n-1} \alpha_3 S_3 L_3 \, l_n'' SL \right] \quad (8).$$

Using expansions (d) on the left and (c) and (d) on the right gives the lengthy form (9).

$$\frac{2}{\sqrt{n-1}} C_1''' = \sum_{S_4 L_4} \sum_{\alpha_3' S_3' L_3'} \sum_{S_5 L_5} [S_1 L_1 \ell'(S_2 L_2)\ell'' SL \,|\, S_1 L_1 \ell'\ell''(S_4 L_4) SL]^* \times$$

$$[\ell^{n-2} \alpha_1 S_1 L_1 \ell_{n-1}' \ell_n''(S_4 L_4) SL \,|\, \frac{e^2}{r_{n,n-1}} \,|\, \ell^{n-2} \alpha_3' S_3' L_3' \ell_{n-1}' \ell_n''(S_5 L_5) SL]$$

$$\times [\ell^{n-2} \alpha_3' S_3' L_3' \ell_n S_3 L_3 \} \ell^{n-1} \alpha_3 S_3 L_3][S_3' L_3' \ell\ell''(S_5 L_5) SL \,|\, S_3' L_3' \ell(S_3 L_3)\ell'' SL] \qquad (9).$$

(9) is simplified by noting that the matrix element reduces to

$$\delta(\alpha_1 S_1 L_1 ; \alpha_3' S_3' L_3') \delta(S_4 L_4) [\ell_{n-1}' \ell_n'' S_4 L_4 \,|\, \frac{e^2}{r_{n,n-1}} \,|\, \ell_{n-1} \ell_n'' S_4 L_4]$$

Thus

$$\frac{2}{\sqrt{n-1}} C_1''' = \sum_{S_4 L_4} [S_1 L_1 \ell'(S_2 L_2)\ell'' SL \,|\, S_1 L_1 \ell'\ell''(S_4 L_4) SL]^*$$

$$[\ell_{n-1}' \ell_n'' S_4 L_4 \,|\, \frac{e^2}{r_{n,n-1}} \,|\, \ell_{n-1} \ell_n'' S_4 L_4] \times$$

$$[\ell^{n-1} \alpha_1 S_1 L_1 \ell S_3 L_3 \} \ell^{n-1} \alpha_3 S_3 L_3][S_1 L_1 \ell\ell''(S_4 L_4) SL \,|\, S_1 L_1 \ell S_3 L_3 \ell'' SL], \qquad (10).$$

Further simplification results by identifying ℓ, ℓ' and ℓ'' with d, s and p electrons respectively. L_4 can then be only a P state. The matrix element occurring in (10) does not depend on spin and can be taken outside the summation sign, as can also the coefficient of fractional parentage. Summation over S_4 gives δ $(S_2\ S_3)$. Denoting

$$R^d = [S_1 p_2 P \,|\, \frac{e^2}{r_{12}} \,|\, d_1 p_2 P] \qquad (11),$$

we obtain

$$C_1'' + C_2'' = R^d \sqrt{n-1} [d^{n-2} \alpha_1 S_1 L_1 d S_3 L_3 \} d^{n-1} \alpha_3 S_3 L_3][4\ d\,p(P)L \,|\, L\ d(L_3)p L] \delta(S_2 S_3)$$

The treatment of C_3''' proceeds in a similar manner. However, the fol-

lowing important differences should be noted. In the first place, $(-1)^{P+Q} = -1$. Taking steps analogous to (7) to (10) we get a result corresponding to (10) in which the direct integral is replaced by minus the exchange integral. Specializing to d, s and p electrons, it is again true that L_4 can only be a P state. However, in the present case it is not true that the matrix element is independent of spin. The singlet and triplet states differ in a minus sign.

$$\left[s_1 p_2\, {}^1P \left| \frac{e^2}{r_{12}} \right| d_2 p_1\, {}^1P\right] = -\left[s_1 p_2\, P \left| \frac{e^2}{r_{12}} \right| d_2 p_1\, P\right] = -R^e$$
$$\left[s_1 p_2\, {}^3P \left| \frac{e^2}{r_{12}} \right| d_2 p_1\, {}^3P\right] = \left[s_1 p_2\, P \left| \frac{e^2}{r_{12}} \right| d_2 p_1\, P\right] = R^e \qquad (12)$$

Accordingly, the summation over S_4 gives the spin dependent factor g^e

$$g^e = \delta(S_1 S)\frac{\left[(2S_2+1)(2S_3+1)\right]^{\frac{1}{2}}}{2S+1} - \delta(S_2 S_3) \qquad (13).$$

The result for C''' accordingly is:

$$C''' = \sqrt{n-1}\left[d^{n-2}\alpha_1 S_1 L_1\, d\, S_3 L_3 \middle\} d^{n-1}\alpha_2 S_2 L_2\right]\left[L_1\, d\,p(P) L \middle| L_1\, d(L_3)\, pL\right] \times \left\{R^d - g^e(\text{spin})\, R^e\right\} \qquad (14).$$

Of course it should be recalled that the quantity of interest is C

$$C = C'' + C''' \quad (C' = 0) \qquad (15).$$

Next we wish to point to what extent the coefficients in the result (14) are available. The coefficients of fractional parentage are listed in R III for the left side of the periodic table. It is a relatively easy matter to calculate the remaining from the listed ones.

The coefficients for coupling the three singular momenta are obtained by means of the W function. It should be noted that there are only 54 such coefficients in the entire iron group (filling of d-shell).

Finally, we wish to state the relationship between the parameters R^d and R^e and the usual Slater integrals. Using the methods of R II it can be shown that

$$R^d = -\tfrac{1}{5}\sqrt{2}\; R^2(sp, dp)$$

$$R^e = -\tfrac{1}{3}\sqrt{2}\; R^1(sp, pd).$$

XVI. A Direct Method for Determining the Transformation Matrix for the Dirac Equation - M. Brachman and M. Hamermesh

In the theory of the Dirac equation, the effect of a space-time transformation is the replacement of the 4-component wave function ψ by $S\psi$ where S is the transformation matrix. Relativistic invariance requires that

$$S^{-1}\gamma^\mu S = a_{\mu\nu}\gamma^\nu \qquad (A)$$

where γ^μ are the Dirac matrices and $a_{\mu\nu}$ is the matrix of the space-time transformation. The calculation of S for given $a_{\mu\nu}$ is usually not done; either one verifies that some S satisfies equation (A) or (cf. Pauli article in Hb. der Physik) one uses properties of continuous groups. The purpose of this note is to give a direct method for solving (A) for the basic space-time transformations.

Taking successive products of the γ's gives 16 independent matrices e^λ, including the identity. The matrix S can be written as $S = \sum_{\lambda=1}^{16} c_\lambda e^\lambda$. The trace of γ^μ is zero, as is that of every e^λ except the identity. Thus, given any equation of the form $\sum p_\lambda e^\lambda = 0$, if we multiply by e^μ and take the trace, we obtain $p_\mu = 0$.

We designate the e^λ for γ^μ by c^μ, for $\gamma^\mu\gamma^\nu$ by $c^{\mu\nu}$, etc., the notation is consistent, since any permutation of the γ's gives a corresponding sign change in the c's. Also $c^{\rho\rho} = c^0$ is the coefficient of the identity matrix.

From equation (A), multiplying successively by γ's and taking the trace, we obtain the following sequence of equations (note that the only summation index is ν):

$$\gamma^\mu S = a_{\mu\nu} S \gamma^\nu \qquad c^\mu = a_{\mu\nu} c^\nu \qquad (1)$$

$$\gamma^\rho\gamma^\mu S = a_{\mu\nu}\gamma^\rho S\gamma^\nu \qquad c^{\mu\rho} = a_{\mu\nu} c^{\rho\nu} \qquad (2)$$

$$\gamma^\sigma\gamma^\rho\gamma^\mu S = a_{\mu\nu}\gamma^\sigma\gamma^\rho S\gamma^\nu \qquad c^{\mu\rho\sigma} = a_{\mu\nu} c^{\rho\sigma\nu} \qquad (3)$$

$$\gamma^\tau\gamma^\sigma\gamma^\rho\gamma^\mu S = a_{\mu\nu}\gamma^\tau\gamma^\sigma\gamma^\rho S\gamma^\nu \qquad c^{\mu\rho\sigma\tau} = a_{\mu\nu} c^{\rho\sigma\tau\nu} \qquad (4)$$

$$S = a_{\mu\nu}\ \gamma^\mu S \gamma^\nu \qquad c^0 = a_{\mu\nu}\ c^{\mu\nu} \qquad (5)$$

$$S\gamma^\rho = a_{\mu\nu}\gamma^\mu S \gamma^\nu\gamma^\rho \qquad c^\rho = a_{\mu\nu}\ c^{\mu\rho\nu} \qquad (6)$$

$$S\gamma^\rho\gamma^\sigma = a_{\mu\nu}\ \gamma^\mu\ S\gamma^\nu\gamma^\rho\gamma^\sigma \qquad c^{\sigma\rho} = a_{\mu\nu}\ c^{\mu\sigma\rho\nu} \qquad (7)$$

I. Time reversal: $a_{11} = a_{22} = a_{33} = 1$, $a_{44} = -1$.

1. Equation 5; set $\mu = 4$. $c^0 = a_{4\nu}\, c^{4\nu} = a_{44}\, c^0 = -c^0$; $\therefore c^0 = 0$.

2. Equation 6; for any ρ, choose $\mu \neq \rho \neq 4$

$$c^\rho = a_{\mu\nu}\ c^{\mu\rho\nu} = a_{\mu\mu}\, c^{\mu\rho\mu} = c^{\mu\rho\mu} = -c^\rho;\ \therefore c^\rho = 0.$$

3. Equation 2; choose $\mu \neq 4 \neq \rho$; $c^{\mu\rho} = a_{\mu\nu}\, c^{\rho\nu} = a_{\mu\mu}\, c^{\rho\mu} = c^{\rho\mu} = -c^{\mu\rho}$;

$$\therefore c^{\mu\rho} = 0$$

(This includes all combinations since ρ can equal 4).

4. Equation 3, with $\mu = 4$ $\rho \neq \sigma \neq 4$;

$$c^{4\rho\sigma} = a_{4\nu}\ c^{\rho\sigma\nu} = a_{44}\, c^{\rho\sigma 4} = -c^{\rho\sigma 4} = -c^{4\rho\sigma};$$

$$\therefore c^{4\rho\sigma} = 0$$

This leaves only $c^{123} \neq 0$.

5. Equation 4, with $\mu = 1, \rho = 2, \sigma = 3, \tau = 4$; $c^{1234} = a_{11}\ c^{2341} = c^{2341}$

$$= -c^{1234} \qquad \therefore c^{1234} = 0$$

Thus $S = \gamma^1\gamma^2\gamma^3$

II. Space inversion: $a_{11} = a_{22} = a_{33} = -1$, $a_{44} = 1$.

1. Equation 5; set $\mu \neq 4$. $c^0 = a_{\mu\nu}\, c^{\mu\nu} = a_{\mu\mu}\ c^0 = -c^0$; $\therefore c^0 = 0$.

2. Equation 6; for any $\rho \neq 4$, set $\mu = 4$; $c^\rho = a_{4\nu}\, c^{4\rho\nu} = a_{44}\, c^{4\rho 4}$

$$= c^{4\rho 4} = -c^\rho; \qquad \therefore c^\rho = 0 \text{ for } \rho \neq 4.$$

3. Equation 2; for $\mu = 4 \neq \rho$; $c^{4\rho} = a_{4\nu}\, c^{\rho\nu} = a_{44}\, c^{\rho 4} = c^{\rho 4} = -c^{4\rho}$

$$\therefore c^{4\rho} = 0.$$

Equation 7; $\rho \neq \sigma \neq 4 \neq \mu$; $c^{\sigma\rho} = a_{\mu\mu}\, c^{\mu\sigma\rho\mu} = -c^{\mu\sigma\rho\mu} = -c^{\sigma\rho}$

so all $c^{\mu\nu} = 0$.

4. Equation 3; $\mu \neq 4$, $\mu \neq \rho \neq \sigma$; $c^{\mu\rho\sigma} = a_{\mu\mu}\, c^{\rho\sigma\mu} = -c^{\rho\sigma\mu} = -c^{\mu\rho\sigma}$;

$$\therefore \text{all } c^{\mu\rho\sigma} = 0.$$

5. Equation 4; $\mu = 4 \neq \rho \neq \sigma \neq \tau$; $c^{4\rho\sigma\tau} = a_{44}\, c^{\rho\sigma\tau 4} = c^{\rho\sigma\tau 4} = -c^{4\rho\sigma\tau} = 0$.

Thus $S = \gamma^4$.

III. Rotation through $\theta \neq \pi$ in xy plane: $a_{11} = a_{22} = \cos\theta$.

$a_{33} = a_{44} = 1 \qquad a_{12} = -a_{21} = \sin\theta$.

1. Equation 6, choose $\mu \neq \rho$, $\mu = 3$ or 4; $c^{\rho} = a_{\mu\mu}\, c^{\mu\rho\mu} = c^{\mu\rho\mu} = -c^{\rho} = 0$.

2. Equation 2, " " " ; $c^{\mu\rho} = a_{\mu\mu}\, c^{\rho\mu} = c^{\rho\mu} = -c^{\mu\rho} = 0$;

thus all $c^{\mu\rho} = 0$ except c^{12}.

3. Equation 6, for $\rho = 3$ or 4, let $\mu = 1$;

$$c^{\rho} = a_{11}\, c^{1\rho 1} + a_{12}\, c^{1\rho 2}$$
$$= -a_{11}\, c^{\rho} + a_{12}\, c^{1\rho 2}$$

since $a_{11} \neq -1$, $a_{12} \neq 0$, and $c^{\rho} = 0$, we get $c^{1\rho 2} = 0$ for $\rho = 3, 4$.

Equation 3 with $\rho = 3$, $\sigma = 4$.

a) $\mu = 1$; $c^{134} = a_{11}\, c^{341} + a_{12}\, c^{342} = a_{11}\, c^{134} + a_{12}\, c^{234}$

b) $\mu = 2$; $c^{234} = a_{21}\, c^{341} + a_{22}\, c^{342} = a_{21}\, c^{134} + a_{22}\, c^{234}$.

These simultaneous equations have only null solutions.

4. Equation 4, $\mu = 4 \neq \rho \neq \sigma \neq \tau$; $c^{4\rho\sigma\tau} = a_{44}\, c^{\rho\sigma\tau 4} = c^{\rho\sigma\tau 4} = -c^{4\rho\sigma\tau} = 0$.

These leave only c^0 and c^{12}.

5. Equation 5, $\mu = 1$; $c^0 = a_{1\nu}\, c^{1\nu} = a_{11}\, c^0 + a_{12}\, c^1$

$$\frac{c^0}{c^1} = \frac{a_{12}}{1-a_{11}} = \frac{\sin\theta}{1-\cos\theta} = \frac{\cos\theta/2}{\sin\theta/2}$$

$$\therefore S = \cos\theta/2 + \gamma^1\gamma^2 \sin\theta/2 = e^{\gamma^1\gamma^2\theta/2}$$

XVII. An Iterative Formula for Approximating an Eigen Value of a Linear Second Order Ordinary Differential Equation R. E. Meyerott and D. A. Flanders

In the course of carrying out numerical calculations of radial wave functions of electrons in atoms one must solve a special case of the following problem: Determine eigen values λ and corresponding eigen functions $S(r)$, twice differentiable over a closed interval $[a,b]$, satisfying the differential equation

$$S'' + (V + \lambda)S = 0, \tag{1A}$$

the boundary conditions

$$S(a) = 0, \tag{1B}$$

$$S(b) = 0, \tag{1C}$$

and the normalizing condition

$$\int_a^b S^2 dr = 1. \tag{1D}$$

We assume that the interval $[a,b]$ and the properties of $V(r)$ in that interval guarantee the existence of a discrete set of eigen values, and that we seek only members of that discrete set. The normalizing condition serves to eliminate the trivial solution $S = 0$ and to determine the scale factor of S uniquely, and so may be replaced by any other condition having like properties.

A commonly used procedure in such cases may be regarded as based on the following considerations: For any fixed value of λ let $L_\lambda(r)$ satisfy (1A) and (1B) in the half-closed interval $[a,b)$, and let $R_\lambda(r)$ satisfy (1A) and (1C) in the half-closed interval (a,b), neither function being identically zero. Let c be a value of r in the open interval (a,b) such that $L_\lambda(c) \neq 0 \neq R_\lambda(c)$. Define $T_\lambda(r)$ by

$$T_\lambda(r) = L_\lambda(r)/L_\lambda(c) \quad \text{for } r \text{ in } [a,c], \tag{2}$$

$$= R_\lambda(r)/R_\lambda(c) \quad \text{for } r \text{ in } [c,b].$$

Since $T_\lambda(c) = 1$, $T_\lambda(r)$ is then a continuous function in $[a, b]$ that can fail to satisfy the requirements of the problem only because it may have a finite jump discontinuity in its first derivative at $r = c$. Note, however, that both left- and right-hand first and second derivatives exist at $r = c$, and that the two second derivatives have the same value at this point, that is that $T''_\lambda(c^-) = L''_\lambda(c)/L_\lambda(c) = R''_\lambda(c)/R_\lambda(c) = T''_\lambda(c^+)$, since both L_λ and R_λ satisfy (1A) in a neighborhood of $r = c$. Thus a necessary and sufficient condition that $T_\lambda(r)$ be an eigen function is that

$$T'_\lambda(c^-) = T'_\lambda(c^+), \tag{3}$$

in other words, that the logarithmic derivatives of L_λ and R_λ be equal at $r = c$. If we denote the difference of these logarithmic derivatives by $D_\lambda(r)$ we may express condition (3) in the form

$$D_\lambda(c) \equiv [L'_\lambda(c)/L_\lambda(c)] - [R'_\lambda(c)/R_\lambda(c)] = 0, \tag{4}$$

in which $D_\lambda(c)$ for fixed c appears as a measure of the closeness of λ to an eigen value.

The application of this condition is made by computing L_λ, R_λ and $D_\lambda(c)$ for various trial values of λ that bracket an eigen value sufficiently closely so that one is sure that not more than one eigen value lies in the range. (This can be assured by keeping track of the number of nodes in T_λ.) By inverse interpolation on λ in equation (4) one may then determine a better estimate of the eigen value. This process may be repeated until the maximum accuracy permitted by the integration procedure is attained.

Since the evaluation of $D_\lambda(c)$ may involve numerical integration of equation (1A) from a to c and from b to c, it is desirable to reduce as much as possible the number of trial values of λ required in the procedure. In many cases the systematic nature of the search for eigen values and possibly information based on the underlying physical problem may make it possible to form a rather good initial estimate of λ. It is the purpose of this note

to show that once a good estimate of λ has been found, a better estimate may ordinarily be found from this value alone by using as a correction to the given value a function $E_\lambda(c)$ closely related to $D_\lambda(c)$. In effect one thus replaces the Rule of False Position by Newton's Method. The function used is simply a "normalized" $D_\lambda(c)$,

$$(5) \qquad E_\lambda(c) = D_\lambda(c) \quad / \quad \int_a^b T_\lambda^2 \, dr.$$

This result is obtained by stating the eigen-value problem in variational terms. Let

$$(6) \qquad I(\lambda, S), = \int_a^b \left[(S')^2 - (V + \lambda) S^2 \right] dr,$$

be the integral to be made stationary, subject to some normalizing side condition equivalent to (1D). As the class of admissible functions we take functions S that are not identically zero in $[a,b]$, that satisfy the boundary conditions (1B) and (1C), and that are continuous and have piecewise continuous first derivatives in $[a,b]$. The eigen functions must then have continuous first and second derivatives in $[a,b]$ and must satisfy the Euler condition, which is precisely the differential equation (1A). Furthermore, if λ_0 and S_0 make $I(\lambda,S)$ stationary, then $I(\lambda_0,S_0) = 0$.

Now assume that λ_0 is a discrete eigen value, that $S_0(r)$ is the corresponding eigen function "normalized" so that $S_0(c) = 1$, that $\lambda \approx \lambda_0$, say $\lambda + \delta\lambda = \lambda_0$, and that $T_\lambda(r)$ is defined as in (2). Set $T_\lambda = S_0 + \delta S$. Then $I(\lambda, T_\lambda) = I(\lambda_0, T_\lambda) + \delta \int_a^b T_\lambda^2 \, dr$. Since by hypothesis $(I\lambda_0, T_\lambda)$ $= I(\lambda_0, S_0) = 0$ to within second order terms in δS and its derivatives,

$$(7) \qquad I(\lambda, T_\lambda) \approx \delta\lambda \int_a^b T^2 dr.$$

On the other hand, integrating by parts, $I(\lambda, T_\lambda) =$

$$\int_a^{c} (T'_\lambda)^2 dr + \int_c^b (T'_\lambda)^2 dr - \int_a^b (V+\lambda) T_\lambda^2 \, dr = T_\lambda T I \Big|_{a}^{c-} + T_\lambda T'_\lambda \Big|_{c+}^{b} -$$

$$\int_a^b \left[T_\lambda T''_\lambda + (V+\lambda) T_\lambda^2 \right] dr = T_\lambda T_\lambda \Big|_{c+}^{c-} - \int_a^b \left[T''_\lambda + (V+\lambda) T_\lambda \right] T_\lambda dr =$$

$T'_\lambda\Big|_{C+}^{C-} = D_\lambda(c)$, since T_λ satisfies the differential equation, is = 0 at $r = a$ and $r = b$, and = 1 at $r = c$. Combining this result with (7) we have

$$\delta \approx D_\lambda(c) \Big/ \int_a^b T_\lambda^2 \, dr = E_\lambda(c). \tag{8}$$

In practice we may assume that L_λ and R_λ have been found by numerical integration to some common mesh point $r = c$. If $r = c+h$ is the next mesh point beyond $r = c$, we need only integrate from a to c+h and from b to c. If we then approximate the derivatives of L_λ and R_λ by first order differences we have

$$D_\lambda(c) = \left[\frac{L_\lambda(c+h)}{L_\lambda(c)} - \frac{R_\lambda(c+h)}{R_\lambda(c)}\right]\Big/h, \tag{9}$$

$$E_\lambda(c) = D_\lambda(c) \Big/ \left\{ \int_a^c \left[L_\lambda(r)/L_\lambda(c)\right]^2 dr - \int_c^b \left[R_\lambda(r)/R_\lambda(c)\right]^2 dr \right\}. \tag{10}$$

The denominator does not change rapidly with λ, and so need usually be computed only once.

The analogy with Newton's method is made more striking by the following observation. In effect we wish to solve the equation $I(\lambda, T_\lambda) = 0$. The correction δ given by Newton's method would be $-I(\lambda, T_\lambda)\big/\left[dI/d\lambda\right]$. If in differentiating I we neglect the contribution of T_λ as a function of λ, then $dI/d\lambda = -\int_a^b T_\lambda^2 \, dr$. This, combined with $I(\lambda, T_\lambda) = D_\lambda(c)$, gives the relation (8).